(Fig. 1). Importantly, this mono-Ub stabilizing effect of UCH-L1 was independent of its enzymatic activity, as the C90S mutant, which lacks enzymatic activity but retains its Ub-interacting ability, still showed a mono-Ub stabilizing effect in cells.

As mentioned earlier, UCH-L1 is a highly expressed protein. Thus, the elucidation of the mechanisms involved in the regulation of UCH-L1 should be an important issue. Recently, a post-translational modification of UCH-L1 that controls the function of UCH-L1 was identified (Meray and Lansbury, 2007). The type of modification is mono-ubiquitination, which may occur reversibly to a lysine residue near the active site (probably K157) of UCH-L1 (Fig. 1). Mono-ubiquitinated UCH-L1, as mimicked by an Ub-UCH-L1 fusion protein, failed to bind mono-Ub and to increase mono-Ub levels in the cell. The enzymatic activity of UCH-L1 may also be inhibited by this modification because it prevents binding to the ubiquitinated targets. In addition, mono-ubiquitinated UCH-L1 was hydrolyzed in intra-molecular manner (Fig. 1). Thus, UCH-L1 might regulate its functional capability by auto-deubiquitination.

In addition to ubiquitination, the existence of a beta-*N*-acetylglucosamine (*O*-GlcNAc)-modified UCH-L1 in the synaptosome fraction of rat brain was reported (Fig. 1) (Cole and Hart, 2001). Moreover, amino-terminally truncated forms of UCH-L1 were found in human brains (Fig. 1), and the levels of this truncated form were shown to be decreased in AD brains but not in PD brains (Choi et al., 2004). Further effort to elucidate the physiological significance of these modifications and their relationship to the pathogenesis of AD and PD should be made.

3. *Gad* mice and the physiological function of UCH-L1 in the brain

Gad mice exhibit an autosomal recessively inherited disorder caused by an in-frame deletion that includes exons 7 and 8 of *Uchl1*, leading to a lack of UCH-L1 expression (Saigoh et al., 1999). These mice show sensory ataxia at an early stage, followed by motor ataxia at a later stage. Pathologically, the mutant is characterized by 'dying-back'-type axonal degeneration and formation of spheroid bodies in nerve terminals. In addition, *gad* mice show abnormal accumulation of APP, β-amyloid (Ichihara et al., 1995), Ub, and proteasome subunit-positive deposits (Saigoh et al., 1999) in the degenerating neuronal axons. These results clearly indicate that UCH-L1 is essential for the functional maintenance of some subsets of neuronal axons.

On the contrary, most neurons show no signs of degeneration in the brains of *gad* mice. By analyzing these neurons in *gad* mice, we found that a lack of UCH-L1 protects cells from acute stress-induced apoptosis (Harada et al., 2004). In wild-type mouse retina, light stimuli and ischemic retinal injury induced strong Ub expression in the inner retina with an expression pattern similar to that of UCH-L1. On the other hand, *gad* mice showed reduced Ub induction after light stimuli and ischemia, whereas the expression levels of anti-apoptotic and pro-survival proteins were significantly higher. Consistently, ischemia-induced caspase activity and neural cell apoptosis were suppressed to ~70% in *gad* mice. The heat-induced apoptosis of testicular cells was also suppressed in *gad* mice (Kwon et al., 2004). These reports demonstrate that UCH-L1 is involved in the regulation of stress-induced apoptosis, presumably through Ub induction.

4. Oxidative modification of UCH-L1 and neurodegeneration

Recently, an increased amount of oxidatively modified UCH-L1 in the brains of AD and PD patients, compared to normal brains, was reported (Castegna et al., 2002; Choi et al., 2004; Butterfield et al., 2006). The oxidative stress may cause such modifications to the protein. At present, several methionine residues and one cysteine residue of UCH-L1 have been reported as possible targets of oxidation; these form methionine sulfoxide and cysteinic acid (Cys–SO_3H), respectively, in PD and AD brains. Furthermore, the level of carbonyl-modified UCH-L1, which is also induced by oxidative stress, was found to be increased in PD and AD brains (Choi et al., 2004).

Consistent with the above data, addition of 4-hydroxy-2-nonenal (HNE; one of the carbonyls) induced the HNE modification of recombinant UCH-L1 *in vitro* (Nishikawa et al., 2003). HNE is an endogenous neurotoxin and a candidate mediator of oxidative stress caused by lipid hyperoxidation, known to trigger the cell death of neurons. In addition, proteins modified by HNE at lysine, histidine and/or cysteine residues are accumulated in the nigral neurons and the Lewy bodies of PD patients (Yoritaka et al., 1996; Castellani et al., 2002) and in the neurofibrillary tangles of AD patients (Montine et al., 1997). Cysteine (C90) and histidine (H161) form the active center of UCH-L1 along with asparagine (N176). Thus, the alteration of UCH-L1 activity was presumed to occur as a result of HNE modification. In agreement with this hypothesis, the hydrolase activities of HNE-modified UCH-L1 were reduced to about 40–80% of non-modified UCH-L1, and were inversely correlated with the degree of modification (Nishikawa et al., 2003). Oxidative stress is now recognized as an important factor, which is implicated in the pathogenesis of a number of age-related neurodegenerative diseases including PD and AD (Halliwell, 2006; Lin and Beal, 2006). Thus, the oxidative modification and subsequent decrease in the enzymatic activity of UCH-L1 may affect the function and survival of neurons, leading to the pathogenesis of AD and PD.

5. Decreased level of UCH-L1 and AD

As mentioned above, UCH-L1 is often present in the Ub-positive inclusions known as neurofibrillary tangles found in AD (Lowe et al., 1990). A recent report indicated that brains from patients with sporadic AD contain decreased levels of soluble UCH-L1, which is inversely proportional to tangle number (Choi et al., 2004). In addition, *gad* mice show an accumulation of amyloid precursor protein (APP) and β-amyloid, typical proteins accumulated in the inclusions of AD brains (Ichihara et al., 1995). Thus, a reduction in the levels of functional UCH-L1 was speculated to contribute to the

pathogenesis of AD. Recently, a group showed that the introduction of UCH-L1 rescued the synaptic and cognitive function of AD model mice (Gong et al., 2006). They used double Tg mice, over-expressing APP together with presenilin 1 (PS1), as an AD mouse model. At a young age following β-amyloid elevation, these mice showed cognitive defects such as inhibition of long-term potentiation (LTP), a type of synaptic plasticity related to memory. The protein level of UCH-L1 was significantly decreased in the hippocampi of these APP/PS1 Tg mice. Remarkably, synaptic function was restored to normal level when UCH-L1 protein fused to the transduction domain of HIV-transactivator protein (TAT) was transduced to hippocampal slices from APP/PS1 Tg mice. In fact, introduction of TAT-UCH-L1 to APP/PS1 mice, over time, improved their contextual learning. This therapeutic effect may be dependent on the enzymatic activity of UCH-L1 because the C90S mutant did not show any significant effect. These findings clearly demonstrate a link between decreased UCH-L1 function and the pathogenesis of AD. Further analysis may prove UCH-L1 to be a useful therapeutic target for treating AD.

6. I93M mutation with gain of toxic function of UCH-L1 and PD

In 1998, a cytosine to guanine (C277G) mutation in the *UCHL1* gene was reported in a German family affected with PD (Leroy et al., 1998). This missense mutation leads to an I93M amino acid substitution in the UCH-L1 protein. In this German family, four out of seven family members were affected with the autosomal dominant form of PD. All of the patients clinically resembled those with sporadic PD. However, there was an unaffected presumed carrier of this mutation in the family. Moreover, gene linkage analysis of *UCHL1* in other PD families failed to discover new families carrying this mutation. Therefore, the link between the I93M mutation in UCH-L1 and the development of PD has been questioned, with the assumption that the C277G alteration in the *UCHL1* gene is a rare polymorphism. To clarify the link between *UCHL1* mutation and PD, a series of experiments, including the *in vitro* biochemical analysis of mutant UCH-L1 and an analysis of Tg mice expressing UCH-L1^{I93M}, were performed.

The analysis of recombinant UCH-L1^{I93M} showed a decrease in its deubiquitinating activity to about 55% of the UCH-L1^{WT} activity level, using the model substrate Ub-amino methyl cumarine (AMC) (Table 1) (Leroy et al., 1998; Nishikawa et al., 2003). However, *gad* mice, which bear no activity of UCH-L1, show no signs of dopaminergic cell loss, the typical pathological hallmarks of PD. In addition, heterozygous mice, which are presumed to show half of the activity level seen in wild-type mice, are asymptomatic (Saigoh et al., 1999). Despite the species difference between mice and humans, these results indicate that the molecular mechanism involved in PD cannot simply be explained by decreased enzymatic activity (Saigoh et al., 1999).

We next compared the secondary structures of UCH-L1^{WT} and UCH-L1^{I93M} using recombinant proteins. Circular dichroism analysis showed that the UCH-L1^{I93M} contains a decreased level of α-helix compared with UCH-L1^{WT} (Table 1) (Nishikawa et al., 2003). It is reported that the SH-SY5Y cells expressing UCH-L1^{I93M} form an increased number of UCH-L1-positive aggregates compared with cells expressing UCH-L1^{WT} or UCH-L1^{C90S}, an enzymatic activity-defective mutant (Ardley et al., 2004). Thus, the I93M mutation may change the conformation of UCH-L1, leading to altered biochemical properties.

To ascertain if the I93M mutation gives rise to a gain of toxic function *in vivo*, we made a transgenic (Tg) mouse expressing UCH-L1^{I93M} (I93M Tg mouse) and analyzed this mouse to determine if UCH-L1^{I93M} could induce dopaminergic neuron loss. The I93M Tg mice showed several pathological changes related to PD (Setsuie et al., 2007). They showed an age-dependent decline in the number of tyrosine hydroxylase (TH)-positive dopaminergic neurons in the substantia nigra. The striatal dopamine content also decreased in parallel with the decrease in the number of dopaminergic neurons. Although we did not find any signs of Lewy body formation, we found silver staining-positive argyrophilic grains and abnormal electron dense core vesicles, which are also found in the autopsied brains of PD patients. In addition, we found aggregates containing both UCH-L1 and Ub in the perinuclei of dopaminergic neurons in the substantia nigra of I93M Tg mice. Therefore, the gain of toxic function caused by the I93M mutation in UCH-L1 might be the main factor contributing to the pathogenesis of PD.

Table 1
Association between UCH-L1 mutants and PD

	WT	I93M	S18Y	References
Incidence of PD		↑	↓	[a]
Functional comparison				
Hydrolase activity	(100%)	↓↓	↑	Leroy et al. (1998), Nishikawa et al. (2003)
Ligase activity	(100%)	↓	↓↓	Liu et al. (2002)
Mono-Ub binding affinity	+	ND	ND	Osaka et al. (2003)
Structural comparison				
α-Helix content	(Normal)	↓	±	Nishikawa et al. (2003), Naito et al. (2006)
Globularity[b]	+	+++	±	Naito et al. (2006)

[a] For references please see the text.
[b] The spherical shape is indicated as ± and the ellipsoidal degree is indicated by +.

7. S18Y polymorphism in UCH-L1 and PD

A polymorphism in UCH-L1 resulting in the amino acid substitution of serine 18 to tyrosine was first reported in 1999 with the possible protective effect against PD (Maraganore et al., 1999). This polymorphism is relatively common in Japanese (allele frequency is 39–54%) and Chinese (~50%) populations, but is rare in European (14–20%) populations (Liu et al., 2002). Further analysis indicated that this inverse association between this polymorphism and PD exists in some populations, such as in Japanese and Chinese but not in others (Maraganore et al., 1999; Mellick and Silburn, 2000; Wintermeyer et al., 2000; Levecque et al., 2001; Wang et al., 2002; Elbaz et al., 2003; Toda et al., 2003; Maraganore et al., 2004; Facheris et al., 2005; Healy et al., 2006; Tan et al., 2006; Carmine Belin et al., 2007). This association was most apparent for younger cases of PD compared with younger controls. In addition, the protection was dependent on the S18Y allele dosage.

A group showed that the Ub ligase activity of UCH-L1, as mentioned above, is responsible for this reduced risk for PD associated with the S18Y polymorphism (Liu et al., 2002). Ub ligase activity of UCH-L1 was shown towards α-synuclein (probably di-ubiquitinated α-synuclein) as a substrate, leading to Ub chain formation (elongation) through lysine 63 of the Ub molecules (Fig. 1). When substrates are poly-ubiquitinated via lysine 63 of Ub, they escape from Ub-proteasomal system (UPS)-dependent protein degradation leading to the stabilization of the substrate. UCH-L1^{WT} tended to form dimers in contrast to UCH-L1^{S18Y}, leading to increased ligase activity in UCH-L1^{WT} (Table 1). Thus, the stability of α-synuclein may be enhanced in the presence of UCH-L1^{WT} compared to UCH-L1^{S18Y}. This difference may reduce the protein level of α-synuclein and reduce the risk of PD in subjects with the S18Y polymorphism. From these experiments, the authors proposed a mechanism in which the ligase activity of UCH-L1 might affect the morbidity of PD in the brain.

Using small angle neutron scattering (SANS), we compared the structural differences that exist between UCH-L1 variants, wild type, I93M and S18Y in aqueous solution (Naito et al., 2006). SANS is an effective method to analyze detailed protein configuration in solution. Using this method, all of the recombinant UCH-L1 variants formed dimers in water. I93M was more ellipsoidal compared with wild-type protein, and S18Y promoted globularity compared with wild-type protein (Table 1). Thus, the shape of the mutant UCH-L1 in water correlated with the risk of PD. Although further analysis should be performed to determine the significance of UCH-L1 dimerization and the S18Y polymorphism for neurodegeneration, the experiments performed in these two laboratories have provided some clues.

8. Concluding remarks and future prospects

UCH-L1 is indicated as a multi-functional protein (Fig. 1) with abundant expression in neurons. In addition, it has become apparent that UCH-L1 may contribute to the pathogenesis of PD and AD. Thus, it is a probable diagnostic and medicinal target of these diseases. However, the mechanism of neurodegeneration induced by I93M mutation and the mechanisms underlying the decreased expression, amino-terminal truncation and increased oxidative modification of UCH-L1 in neurodegenerative diseases have yet to be revealed. In addition, there are several unresolved issues regarding the molecular functions and regulation of UCH-L1. The *in vivo* substrates need to be defined. The ways in which the function and localization of UCH-L1 are regulated are largely unknown. The identification and the analysis of the interacting partners might give us some clues, one of which is Jun activation domain binding protein (JAB1) in H1299 cell, a lung cancer cell line (Fig. 1) (Caballero et al., 2002), though their interaction in the brain is unknown. Recently, a physiological function of an isozyme UCH-L3 was identified in the oxidative stress-induced apoptosis of photoreceptor cells, neurons that reside in the retina (Semenova et al., 2003; Sano et al., 2006). In addition, a reciprocal function of UCH-L1 and UCH-L3 has been proposed in the heat stress-induced apoptosis of testis in mice (Kwon et al., 2004). Thus, the functional diversity between UCH-L1 and UCH-L3 should also be defined. In addition to neurodegeneration, UCH-L1 is thought to be involved in the regulation of ATP receptors in neurons (Manago et al., 2005), in the morphology of neuronal precursors (Sakurai et al., 2006), in the normal function of the testis and the ovary (Kwon et al., 2005; Sekiguchi et al., 2006) and in various human diseases such as cancer (Hibi et al., 1999). Thus, UCH-L1 might contribute to more diverse phenomena than were previously thought.

Acknowledgements

The authors thank Dr. Tomohiro Kabuta and Dr. Satoshi Nagamine for their helpful comments. This work was supported in part by Grants-in-Aid for Scientific Research from the Ministry of Health, Labour and Welfare of Japan, Grants-in-Aid for Scientific Research from the Ministry of Education, Culture, Sports, Science and Technology of Japan, the Program for Promotion of Fundamental Studies in Health Sciences of the National Institute of Biomedical Innovation, and a grant from Japan Science and Technology Agency.

References

Ardley, H.C., Scott, G.B., Rose, S.A., Tan, N.G., Robinson, P.A., 2004. UCH-L1 aggresome formation in response to proteasome impairment indicates a role in inclusion formation in Parkinson's disease. J. Neurochem. 90, 379–391.

Butterfield, D.A., Gnjec, A., Poon, H.F., Castegna, A., Pierce, W.M., Klein, J.B., Martins, R.N., 2006. Redox proteomics identification of oxidatively modified brain proteins in inherited Alzheimer's disease: an initial assessment. J. Alzheimers Dis. 10, 391–397.

Caballero, O.L., Resto, V., Patturajan, M., Meerzaman, D., Guo, M.Z., Engles, J., Yochem, R., Ratovitski, E., Sidransky, D., Jen, J., 2002. Interaction and colocalization of PGP9.5 with JAB1 and p27(Kip1). Oncogene 21, 3003–3010.

Carmine Belin, A., Westerlund, M., Bergman, O., Nissbrandt, H., Lind, C., Sydow, O., Galter, D., 2007. S18Y in ubiquitin carboxy-terminal hydrolase L1 (UCH-L1) associated with decreased risk of Parkinson's disease in Sweden. Parkinsonism Relat. Disord. 13, 295–298.

Castegna, A., Aksenov, M., Thongboonkerd, V., Klein, J.B., Pierce, W.M., Booze, R., Markesbery, W.R., Butterfield, D.A., 2002. Proteomic identification of oxidatively modified proteins in Alzheimer's disease brain. Part II: Dihydropyrimidinase-related protein 2, alpha-enolase and heat shock cognate 71. J. Neurochem. 82, 1524–1532.

Castellani, R.J., Perry, G., Siedlak, S.L., Nunomura, A., Shimohama, S., Zhang, J., Montine, T., Sayre, L.M., Smith, M.A., 2002. Hydroxynonenal adducts indicate a role for lipid peroxidation in neocortical and brainstem Lewy bodies in humans. Neurosci. Lett. 319, 25–28.

Choi, J., Levey, A.I., Weintraub, S.T., Rees, H.D., Gearing, M., Chin, L.S., Li, L., 2004. Oxidative modifications and down-regulation of ubiquitin carboxyl-terminal hydrolase L1 associated with idiopathic Parkinson's and Alzheimer's diseases. J. Biol. Chem. 279, 13256–13264.

Cole, R.N., Hart, G.W., 2001. Cytosolic *O*-glycosylation is abundant in nerve terminals. J. Neurochem. 79, 1080–1089.

Das, C., Hoang, Q.Q., Kreinbring, C.A., Luchansky, S.J., Meray, R.K., Ray, S.S., Lansbury, P.T., Ringe, D., Petsko, G.A., 2006. Structural basis for conformational plasticity of the Parkinson's disease-associated ubiquitin hydrolase UCH-L1. Proc. Natl. Acad. Sci. U.S.A. 103, 4675–4680.

Elbaz, A., Levecque, C., Clavel, J., Vidal, J.S., Richard, F., Correze, J.R., Delemotte, B., Amouyel, P., Alperovitch, A., Chartier-Harlin, M.C., Tzourio, C., 2003. S18Y polymorphism in the UCH-L1 gene and Parkinson's disease: evidence for an age-dependent relationship. Mov. Disord. 18, 130–137.

Facheris, M., Strain, K.J., Lesnick, T.G., de Andrade, M., Bower, J.H., Ahlskog, J.E., Cunningham, J.M., Lincoln, S., Farrer, M.J., Rocca, W.A., Maraganore, D.M., 2005. UCHL1 is associated with Parkinson's disease: a case-unaffected sibling and case-unrelated control study. Neurosci. Lett. 381, 131–134.

Gong, B., Cao, Z., Zheng, P., Vitolo, O.V., Liu, S., Staniszewski, A., Moolman, D., Zhang, H., Shelanski, M., Arancio, O., 2006. Ubiquitin hydrolase Uch-L1 rescues beta-amyloid-induced decreases in synaptic function and contextual memory. Cell 126, 775–788.

Halliwell, B., 2006. Oxidative stress and neurodegeneration: where are we now? J. Neurochem. 97, 1634–1658.

Harada, T., Harada, C., Wang, Y.L., Osaka, H., Amanai, K., Tanaka, K., Takizawa, S., Setsuie, R., Sakurai, M., Sato, Y., Noda, M., Wada, K., 2004. Role of ubiquitin carboxy terminal hydrolase-L1 in neural cell apoptosis induced by ischemic retinal injury in vivo. Am. J. Pathol. 164, 59–64.

Healy, D.G., Abou-Sleiman, P.M., Casas, J.P., Ahmadi, K.R., Lynch, T., Gandhi, S., Muqit, M.M., Foltynie, T., Barker, R., Bhatia, K.P., Quinn, N.P., Lees, A.J., Gibson, J.M., Holton, J.L., Revesz, T., Goldstein, D.B., Wood, N.W., 2006. UCHL-1 is not a Parkinson's disease susceptibility gene. Ann. Neurol. 59, 627–633.

Hibi, K., Westra, W.H., Borges, M., Goodman, S., Sidransky, D., Jen, J., 1999. PGP9.5 as a candidate tumor marker for non-small-cell lung cancer. Am. J. Pathol. 155, 711–715.

Ichihara, N., Wu, J., Chui, D.H., Yamazaki, K., Wakabayashi, T., Kikuchi, T., 1995. Axonal degeneration promotes abnormal accumulation of amyloid beta-protein in ascending gracile tract of gracile axonal dystrophy (GAD) mouse. Brain Res. 695, 173–178.

Kwon, J., Mochida, K., Wang, Y.L., Sekiguchi, S., Sankai, T., Aoki, S., Ogura, A., Yoshikawa, Y., Wada, K., 2005. Ubiquitin C-terminal hydrolase L-1 is essential for the early apoptotic wave of germinal cells and for sperm quality control during spermatogenesis. Biol. Reprod. 73, 29–35.

Kwon, J., Wang, Y.L., Setsuie, R., Sekiguchi, S., Sato, Y., Sakurai, M., Noda, M., Aoki, S., Yoshikawa, Y., Wada, K., 2004. Two closely related ubiquitin C-terminal hydrolase isozymes function as reciprocal modulators of germ cell apoptosis in cryptorchid testis. Am. J. Pathol. 165, 1367–1374.

Larsen, C.N., Krantz, B.A., Wilkinson, K.D., 1998. Substrate specificity of deubiquitinating enzymes: ubiquitin C-terminal hydrolases. Biochemistry 37, 3358–3368.

Leroy, E., Boyer, R., Auburger, G., Leube, B., Ulm, G., Mezey, E., Harta, G., Brownstein, M.J., Jonnalagada, S., Chernova, T., Dehejia, A., Lavedan, C., Gasser, T., Steinbach, P.J., Wilkinson, K.D., Polymeropoulos, M.H., 1998. The ubiquitin pathway in Parkinson's disease. Nature 395, 451–452.

Levecque, C., Destee, A., Mouroux, V., Becquet, E., Defebvre, L., Amouyel, P., Chartier-Harlin, M.C., 2001. No genetic association of the ubiquitin carboxy-terminal hydrolase-L1 gene S18Y polymorphism with familial Parkinson's disease. J. Neural. Transm. 108, 979–984.

Lin, M.T., Beal, M.F., 2006. Mitochondrial dysfunction and oxidative stress in neurodegenerative diseases. Nature 443, 787–795.

Liu, Y., Fallon, L., Lashuel, H.A., Liu, Z., Lansbury Jr., P.T., 2002. The UCH-L1 gene encodes two opposing enzymatic activities that affect alpha-synuclein degradation and Parkinson's disease susceptibility. Cell 111, 209–218.

Lowe, J., McDermott, H., Landon, M., Mayer, R.J., Wilkinson, K.D., 1990. Ubiquitin carboxyl-terminal hydrolase (PGP9.5) is selectively present in ubiquitinated inclusion bodies characteristic of human neurodegenerative diseases. J. Pathol. 161, 153–160.

Manago, Y., Kanahori, Y., Shimada, A., Sato, A., Amano, T., Sato-Sano, Y., Setsuie, R., Sakurai, M., Aoki, S., Wang, Y.L., Osaka, H., Wada, K., Noda, M., 2005. Potentiation of ATP-induced currents due to the activation of P2X receptors by ubiquitin carboxy-terminal hydrolase L1. J. Neurochem. 92, 1061–1072.

Maraganore, D.M., Farrer, M.J., Hardy, J.A., Lincoln, S.J., McDonnell, S.K., Rocca, W.A., 1999. Case-control study of the ubiquitin carboxy-terminal hydrolase L1 gene in Parkinson's disease. Neurology 53, 1858–1860.

Maraganore, D.M., Lesnick, T.G., Elbaz, A., Chartier-Harlin, M.C., Gasser, T., Kruger, R., Hattori, N., Mellick, G.D., Quattrone, A., Satoh, J., Toda, T., Wang, J., Ioannidis, J.P., de Andrade, M., Rocca, W.A., 2004. UCHL1 is a Parkinson's disease susceptibility gene. Ann. Neurol. 55, 512–521.

Mellick, G.D., Silburn, P.A., 2000. The ubiquitin carboxy-terminal hydrolase-L1 gene S18Y polymorphism does not confer protection against idiopathic Parkinson's disease. Neurosci. Lett. 293, 127–130.

Meray, R.K., Lansbury Jr., P.T., 2007. Reversible monoubiquitination regulates the Parkinson's disease-associated ubiquitin hydrolase UCH-L1. J. Biol. Chem. 282, 10567–10575.

Montine, K.S., Olson, S.J., Amarnath, V., Whetsell Jr., W.O., Graham, D.G., Montine, T.J., 1997. Immunohistochemical detection of 4-hydroxy-2-nonenal adducts in Alzheimer's disease is associated with inheritance of APOE4. Am. J. Pathol. 150, 437–443.

Naito, S., Mochizuki, H., Yasuda, T., Mizuno, Y., Furusaka, M., Ikeda, S., Adachi, T., Shimizu, H.M., Suzuki, J., Fujiwara, S., Okada, T., Nishikawa, K., Aoki, S., Wada, K., 2006. Characterization of multimetric variants of ubiquitin carboxyl-terminal hydrolase L1 in water by small-angle neutron scattering. Biochem. Biophys. Res. Commun. 339, 717–725.

Nijman, S.M., Luna-Vargas, M.P., Velds, A., Brummelkamp, T.R., Dirac, A.M., Sixma, T.K., Bernards, R., 2005. A genomic and functional inventory of deubiquitinating enzymes. Cell 123, 773–786.

Nishikawa, K., Li, H., Kawamura, R., Osaka, H., Wang, Y.L., Hara, Y., Hirokawa, T., Manago, Y., Amano, T., Noda, M., Aoki, S., Wada, K., 2003. Alterations of structure and hydrolase activity of parkinsonism-associated human ubiquitin carboxyl-terminal hydrolase L1 variants. Biochem. Biophys. Res. Commun. 304, 176–183.

Osaka, H., Wang, Y.L., Takada, K., Takizawa, S., Setsuie, R., Li, H., Sato, Y., Nishikawa, K., Sun, Y.J., Sakurai, M., Harada, T., Hara, Y., Kimura, I., Chiba, S., Namikawa, K., Kiyama, H., Noda, M., Aoki, S., Wada, K., 2003. Ubiquitin carboxy-terminal hydrolase L1 binds to and stabilizes monoubiquitin in neuron. Hum. Mol. Genet. 12, 1945–1958.

Saigoh, K., Wang, Y.L., Suh, J.G., Yamanishi, T., Sakai, Y., Kiyosawa, H., Harada, T., Ichihara, N., Wakana, S., Kikuchi, T., Wada, K., 1999. Intragenic deletion in the gene encoding ubiquitin carboxy-terminal hydrolase in gad mice. Nat. Genet. 23, 47–51.

Sakurai, M., Ayukawa, K., Setsuie, R., Nishikawa, K., Hara, Y., Ohashi, H., Nishimoto, M., Abe, T., Kudo, Y., Sekiguchi, M., Sato, Y., Aoki, S., Noda, M., Wada, K., 2006. Ubiquitin C-terminal hydrolase L1 regulates the morphology of neural progenitor cells and modulates their differentiation. J. Cell Sci. 119, 162–171.

Sano, Y., Furuta, A., Setsuie, R., Kikuchi, H., Wang, Y.L., Sakurai, M., Kwon, J., Noda, M., Wada, K., 2006. Photoreceptor cell apoptosis in the retinal degeneration of Uchl3-deficient mice. Am. J. Pathol. 169, 132–141.

Sekiguchi, S., Kwon, J., Yoshida, E., Hamasaki, H., Ichinose, S., Hideshima, M., Kuraoka, M., Takahashi, A., Ishii, Y., Kyuwa, S., Wada, K., Yoshikawa, Y., 2006. Localization of ubiquitin C-terminal hydrolase L1 in mouse ova and its function in the plasma membrane to block polyspermy. Am. J. Pathol. 169, 1722–1729.

Semenova, E., Wang, X., Jablonski, M.M., Levorse, J., Tilghman, S.M., 2003. An engineered 800 kilobase deletion of Uchl3 and Lmo7 on mouse

chromosome 14 causes defects in viability, postnatal growth and degeneration of muscle and retina. Hum. Mol. Genet. 12, 1301–1312.

Setsuie, R., Wang, Y.L., Mochizuki, H., Osaka, H., Hayakawa, H., Ichihara, N., Li, H., Furuta, A., Sano, Y., Sun, Y.J., Kwon, J., Kabuta, T., Yoshimi, K., Aoki, S., Mizuno, Y., Noda, M., Wada, K., 2007. Dopaminergic neuronal loss in transgenic mice expressing the Parkinson's disease-associated UCH-L1 I93M mutant. Neurochem. Int. 50, 119–129.

Tan, E.K., Puong, K.Y., Fook-Chong, S., Chua, E., Shen, H., Yuen, Y., Pavanni, R., Wong, M.C., Puvan, K., Zhao, Y., 2006. Case-control study of UCHL1 S18Y variant in Parkinson's disease. Mov. Disord. 21, 1765–1768.

Toda, T., Momose, Y., Murata, M., Tamiya, G., Yamamoto, M., Hattori, N., Inoko, H., 2003. Toward identification of susceptibility genes for sporadic Parkinson's disease. J. Neurol. 250 (Suppl. 3), III40–III43.

Wang, J., Zhao, C.Y., Si, Y.M., Liu, Z.L., Chen, B., Yu, L., 2002. ACT and UCH-L1 polymorphisms in Parkinson's disease and age of onset. Mov. Disord. 17, 767–771.

Wilkinson, K.D., Lee, K.M., Deshpande, S., Duerksen-Hughes, P., Boss, J.M., Pohl, J., 1989. The neuron-specific protein PGP9.5 is a ubiquitin carboxyl-terminal hydrolase. Science 246, 670–673.

Wilson, P.O., Barber, P.C., Hamid, Q.A., Power, B.F., Dhillon, A.P., Rode, J., Day, I.N., Thompson, R.J., Polak, J.M., 1988. The immunolocalization of protein gene product 9.5 using rabbit polyclonal and mouse monoclonal antibodies. Br. J. Exp. Pathol. 69, 91–104.

Wintermeyer, P., Kruger, R., Kuhn, W., Muller, T., Woitalla, D., Berg, D., Becker, G., Leroy, E., Polymeropoulos, M., Berger, K., Przuntek, H., Schols, L., Epplen, J.T., Riess, O., 2000. Mutation analysis and association studies of the UCHL1 gene in German Parkinson's disease patients. Neuroreport 11, 2079–2082.

Yoritaka, A., Hattori, N., Uchida, K., Tanaka, M., Stadtman, E.R., Mizuno, Y., 1996. Immunohistochemical detection of 4-hydroxynonenal protein adducts in Parkinson disease. Proc. Natl. Acad. Sci. U.S.A. 93, 2696–2701.

Available online at www.sciencedirect.com
ScienceDirect
Bioorganic & Medicinal Chemistry
ELSEVIER
Bioorganic & Medicinal Chemistry 15 (2007) 6810–6818

Identification of novel chemical inhibitors for ubiquitin C-terminal hydrolase-L3 by virtual screening

Kazunori Hirayama,[a,b] Shunsuke Aoki,[b,*] Kaori Nishikawa,[b] Takashi Matsumoto[a] and Keiji Wada[b]

[a]*Department of Electrical Engineering and Bioscience, Graduate School of Advanced Science and Engineering, Waseda University, 3-4-1 Okubo, Shinjuku-ku, Tokyo 169-8555, Japan*
[b]*Department of Degenerative Neurological Diseases, National Institute of Neuroscience, National Center of Neurology and Psychiatry, 4-1-1 Ogawa-Higashi, Kodaira, Tokyo 187-8502, Japan*

Received 11 May 2007; revised 14 July 2007; accepted 18 July 2007
Available online 19 August 2007

Abstract—UCH-L3 (ubiquitin C-terminal hydrolase-L3) is a de-ubiquitinating enzyme that is a component of the ubiquitin–proteasome system and known to be involved in programmed cell death. A previous study of high-throughput drug screening identified an isatin derivative as a UCH-L3 inhibitor. In this study, we attempted to identify a novel inhibitor with a different structural basis. We performed in silico structure-based drug design (SBDD) using human UCH-L3 crystal structure data (PDB code; 1XD3) and the virtual compound library (ChemBridge CNS-Set), which includes 32,799 chemicals. By a two-step virtual screening method using DOCK software (first screening) and GOLD software (second screening), we identified 10 compounds with GOLD scores of over 60. To address whether these compounds exhibit an inhibitory effect on the de-ubiquitinating activity of UCH-L3, we performed an enzymatic assay using ubiquitin-7-amido-4-methylcoumarin (Ub-AMC) as the substrate. As a result, we identified three compounds with similar basic dihydro-pyrrole skeletons as UCH-L3 inhibitors. These novel compounds may be useful for the research of UCH-L3 function, and in drug development for UCH-L3-associated diseases.

1. Introduction

The ubiquitin–proteasome system is responsible for the regulation of cellular proteolysis. In this system, ubiquitination serves as a targeting signal for proteolysis.[1] Ubiquitin C-terminal hydrolase-L3 (UCH-L3) is one of the components of the ubiquitin–proteasome system and hydrolyzes ubiquitin C-terminal adducts for the recycling of cellular ubiquitin.[2] Ubiquitin with C-terminal adducts is a substrate for UCH-L3, and ubiquitin with a free C-terminus is recycled within the ubiquitin–proteasome system. There is some evidence that UCH-L3 plays an important role in programmed cell death. Programmed cell death is implicated in a number of human diseases, including neurodegenerative disease,[3] autoimmune disease,[4] cancers[5,6], etc. Loss of UCH-L3 leads to programmed cell death by apoptosis of certain type of cells in vivo, germ line cells and photoreceptor cells.[7,8] High-level expression of UCH-L3 genes and proteins, and acceleration of UCH-L3 enzymatic activity is reported in multiple types of cancer cells,[5,6] suggesting that UCH-L3 activity may be required for cancer cell survival. Therefore, UCH-L3 is a potential target for drug development to control programmed cell death in specific types of cells including cancer cells.

Structure-based drug design (SBDD) is a method used to discover novel leads for drug development as it enables more rapid hit identification than the classical screening methods of in vitro or in vivo biological assays. The computer-based approach for drug screening, using molecular docking, is a shortcut method when the crystal structure of a target protein is available. Key methodologies for docking small molecules to protein were developed during the early 1980s,[9] and various types of docking simulation software are now available, for example, DOCK,[10] GOLD, and FlexX.[11] BCR-ABL tyrosine kinase inhibitors (IC_{50} values ranging from 10 to 200 μM) were successfully

Keywords: UCH-L3; Dihydro-pyrrole; Structure-based drug design; Virtual screening.
* Corresponding author. Tel.: +81 42 341 2712x5144; fax: +81 42 346 1745; e-mail: aokis@ncnp.go.jp

0968-0896/$ - see front matter © 2007 Elsevier Ltd. All rights reserved.
doi:10.1016/j.bmc.2007.07.016

identified by virtual screening of 200,000 compounds against crystal structures using DOCK,[12] implemented by the anchor-and-grow algorithm with respect to ligand flexibility.[10] Human thymidine phosphorylase inhibitor (IC_{50} = 77 μM) was also identified by virtual screening of 250,521 compounds using DOCK.[13] Furthermore, metallo-β-lactamase inhibitors (IC_{50} values less than 15 μM) were identified through virtual screening by GOLD,[14] using the genetic algorithm for ligand flexibility.

The advantage of chaining different docking programs was evaluated and the results suggested that virtual ligand screening is performed faster with reasonable accuracy by using chained screening, than by using a single program with default parameters.[15] In this study, the results of chained docking against UCH-L3 crystal structure were examined by UCH-L3 hydrolysis activity assay to validate the efficacy of the DOCK–GOLD SBDD method. We identified three inhibitors (IC_{50} = 100–150 μM) of UCH-L3 by the DOCK–GOLD virtual screening of 32,799 compounds.

2. Results and discussion

2.1. Protein preparation and chemical database

In the 3D structure of the UCH-L3-ubiquitin complex, ubiquitin C-terminus is buried in the active site cleft among four active site residues of UCH-L3: Gln89, Cys95, His169, and Asp184.[16,17] During the virtual screening process by DOCK and GOLD, the protein–ligand interacting site was restricted to the binding site of the three ubiquitin C-terminal amino residues (as described in Section 4), in order that the outcome could be verified by a ubiquitin C-terminal hydrolase enzymatic assay. The first DOCK screening was performed against 32,799 compounds of CNS-Set, which was prefiltered by RPBS under the most modest filtering condition.[18]

2.2. DOCK and GOLD screenings

To screen for compounds that bind to the active site, the first screening was performed by DOCK, and the protein–ligand interaction area was restricted to the ubiquitin binding site of UCH-L3 (see Section 4). The top-scoring 1780 compounds (5.4% of the initial 32,799 compounds) with energy scores of less than −30 kcal/mol were selected for further screening. These compounds were then re-screened by GOLD twice, with different genetic algorithm (GA) settings. To predict binding ability to the active site cleft accurately, the protein–ligand interacting area was defined in approximately the same way as in the first DOCK screening step (see Section 4). Screening by GOLD consisted of two rounds. Using the GOLD score, we initially extracted the top scoring 100 compounds from 1780 compounds, using the 7–8 times speed-up GA parameter settings. These 100 compounds were then re-scored using the default GA settings (see Section 4) to more accurately predict binding ability. Ten compounds with GOLD scores of over 60 were predicted to bind to the UCH-L3 active site; that is, 0.03% of the total number of chemical compounds was screened.

2.3. IC_{50} determination

A previous study demonstrated that compounds with GOLD scores of about 60 may inhibit enzyme activity with IC_{50} values of 10–100 μM.[19] An enzyme assay was performed among the top 10 chemicals to address whether they actually bind to the UCH-L3 active site with the predicted affinities (Table 1 and Fig. 1).

Ubiquitin-7-amido-4-methylcoumarin (Ub-AMC; AMC attaches to the carboxyl terminus of ubiquitin) is a fluorogenic substrate of UCH-L3 and other UCH isozymes. UCH-L3 is known to hydrolyze Ub-AMC into free ubiquitin and AMC,[20,21] and the hydrolyzed AMC group is excited at light wavelength of 355 nm and emits fluorescence at 460 nm. Hydrolysis activity of UCH-L3 is inhibited if a compound binds to its active site and thus blocks interaction between the active site of UCH-L3 and the ubiquitin C-terminus. Inhibition of hydrolysis of Ub-AMC leads to a lower concentration of free AMC and hence a lower level of fluorescence intensity.

We experimentally determined the affinity constant (K_m) of Ub-AMC hydrolysis by human UCH-L3 as 83.3 ± 1.5 nM (mean ± SEM, from three independent experiments). The candidate compounds identified by

Table 1. GOLD scores of the top 10 ranked chemicals after GOLD calculation[a]

Docking rank/Compound No.	Compound name	GOLD scores
1	1-Benzyl-3-hydroxy-4-(5-methyl-2-furoyl)-5-(3-pyridinyl)-1,5-dihydro-2*H*-pyrrol-2-one	66.01
2	3-[4-Methyl-5-({[3-(2-thienyl)-1,2,4-oxadiazol-5-yl]methyl}thio)-4*H*-1,2,4-triazol-3-yl]-1*H*-indole	65.62
3	*N*-{4-[1-(2-Furoyl)-5-(2-furyl)-4,5-dihydro-1*H*-pyrazol-3-yl]phenyl}methanesulfonamide	64.85
4	N^1-Cyclopropyl-N^2-(4-methoxyphenyl)-N^2-[(4-methylphenyl)sulfonyl]glycinamide	64.76
5	*N*-{3-[1-Acetyl-5-(2-thienyl)-4,5-dihydro-1*H*-pyrazol-3-yl]phenyl}ethanesulfonamide	64.23
6	3-Hydroxy-5-(4-methoxyphenyl)-1-(1,3,4-thiadiazol-2-yl)-4-(2-thienylcarbonyl)-1,5-dihydro-2*H*-pyrrol-2-one	62.96
7	5-(4-Fluorophenyl)-3-hydroxy-4-(5-methyl-2-furoyl)-1-(3-pyridinylmethyl)-1,5-dihydro-2*H*-pyrrol-2-one	62.73
8	N^1-Cyclopropyl-N^2-[(4-methoxyphenyl)sulfonyl]-N^2-(4-methylphenyl)glycinamide	62.52
9	N^1-Cyclopentyl-N^2-(3-methoxyphenyl)-N^2-(phenylsulfonyl)glycinamide	62.39
10	4-({[5-(2-Furyl)-4-phenyl-4*H*-1,2,4-triazol-3-yl]thio}methyl)-1,3-thiazol-2-amine	62.35

[a] Ten compounds are listed according to the top 10 rank of GOLD scores and assigned the number corresponding to GOLD score ranks.

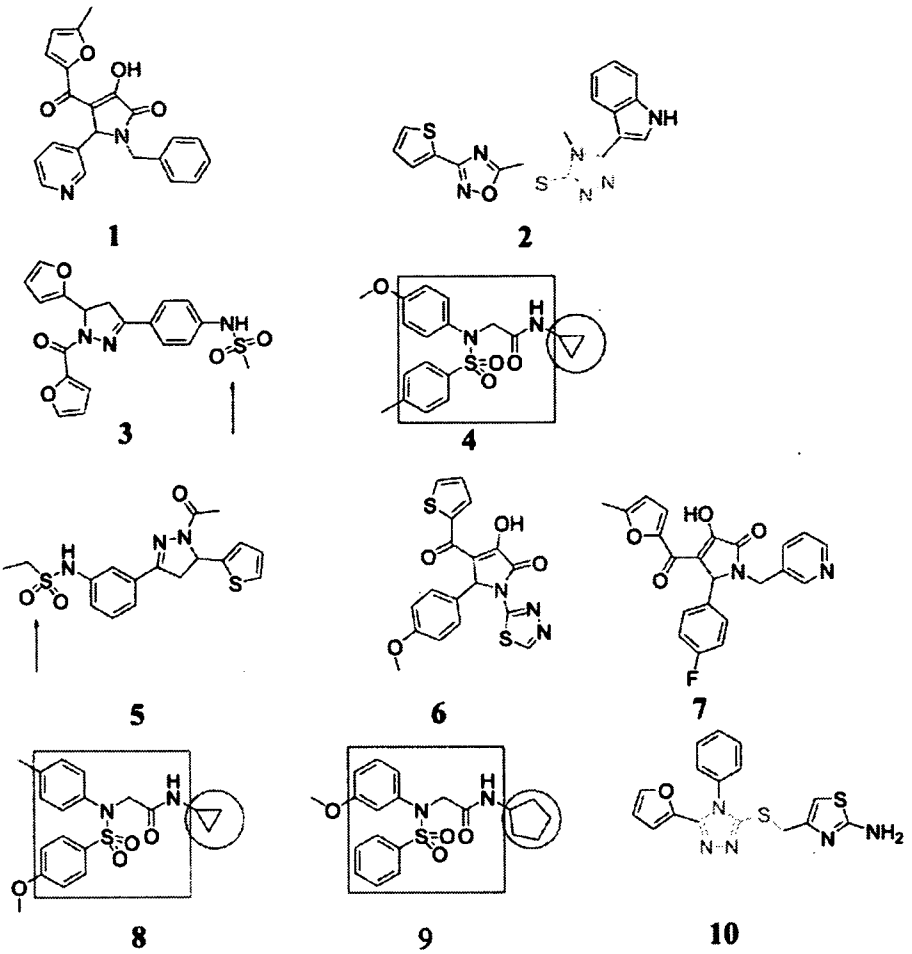

Figure 1. Top 10 ranked compounds identified by DOCK and GOLD screening. Note that there are several shared basic skeletons and functional groups: 1,5-dihydro-2*H*-pyrrol-2-one (drawn in red, compounds **1**, **6**, and **7**), glycinamide (boxed in red, compounds **4**, **8**, and **9**), cycloalkane group (circled in red, compounds **4** and **8**; cyclopropyl, compound **9**; cyclopentyl), 4,5-dihydro-1*H*-pyrazol-3-yl phenyl (drawn in blue, compounds **3** and **5**), sulfonamide (pointed, compounds **3** and **5**), and 4*H*-1,2,4-triazol-3-yl (drawn in green, compounds **2** and **10**).

DOCK–GOLD chained docking screening were tested for their ability to inhibit the hydrolysis activity of UCH-L3, at the Ub-AMC concentration equivalent to the K_m value. Four compounds among these candidates inhibited enzyme activity (Fig. 2a). We did not test the inhibitory effects of compound **3**, as it is a fluorogenic chemical with an emission wavelength of 460 nm. Compounds **1**, **6**, and **7** significantly inhibited the hydrolysis activity of UCH-L3 (initial velocity of Ub-AMC hydrolysis; nM/s [Fig. 2b]). Compounds **1** (401 μM), **6** (375 μM), and **7** (350 μM) inhibited the hydrolysis activity by 83.2 ± 1.5%, 76.5 ± 0.6%, and 76.8 ± 1.0%, respectively, as compared with control DMSO ($p < 0.01$, vs control; Dunnett's test). The IC_{50} value of compound **2** should hypothetically be several hundred μM. Although compound **2** (380 μM) inhibited hydrolysis activity by 16.2 ± 2.1% as compared with control DMSO, the difference was not found to be significant by Dunnett's test. Five other compounds were unable to inhibit the UCH-L3 hydrolysis activity: compound **4** (334 μM; final concentration), compound **5** (331 μM), compound **8** (401 μM), compound **9** (386 μM), and compound **10** (387 μM) (Fig. 2b). Experimentally determined IC_{50} values of compounds **1**, **6**, and **7** (Fig. 3) were as follows: compound **1** (103 μM), compound **6** (154 μM), and compound **7** (123 μM).

2.4. Competitive inhibitor

To show that the identified compounds bind to the active site of the UCH-L3, various concentrations of compound **1** and iodoacetamide (108 mM) were added to UCH-L3/Ub-AMC reaction buffer. Iodoacetamide is a non-competitive inhibitor of UCH-L3 (Fig. 4a). It is a thiol alkylating agent of the UCH-L family and derivatizes and inactivates the active site leading to loss of UCH-L3 enzymatic activity.[22] In the presence of compound **1** and iodoacetamide, the percentage of active UCH-L3 reduced by iodoacetamide treatment was recovered in comparison with the control, and the recovery was dependent on the concentration of compound **1** (Fig. 4b). Our results showed that compound **1** is a competitive inhibitor of UCH-L3. This suggests that compound **1** bound to the UCH-L3 active site to prevent iodoacetamide from inactivating it.

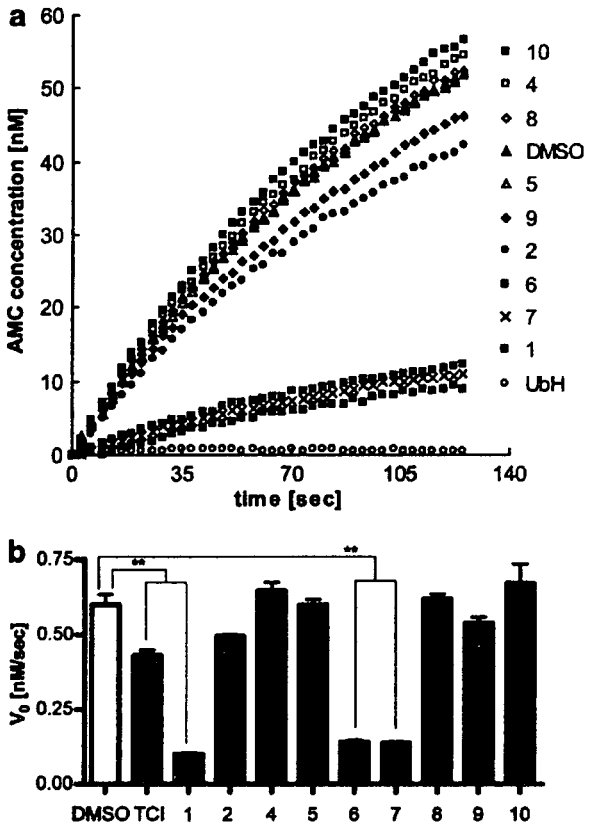

Figure 2. Analysis of UCH-L3 inhibitory effects of compounds **1**–**10**. (a) Kinetics of UCH-L3-catalyzed hydrolysis of Ub-AMC with the compounds. Fluorescence intensity was converted to AMC concentration by subtracting the intensity of fully hydrolyzed substrate from that of solution without substrate. Concentrations of compounds are as follows: compound **1** (401 μM); compound **2** (380 μM); compound **4** (334 μM); compound **5** (331 μM); compound **6** (375 μM); compound **7** (350 μM); compound **8** (401 μM); compound **9** (386 μM); and compound **10** (387 μM). As a known inhibitor, ubiquitin-aldehyde (Ub-H, 120 nM) was used. Each value represents the mean of three independent experiments. (b) Inhibitory effects of compounds on initial velocity of hydrolysis (V_0) are shown. Fluorescence intensity was converted by the same method described in (a). 4,5,6,7-Tetrachloroindan-1,3-dione (TCI, 20 μM) was used as a UCH-L3 selective inhibitor with IC_{50} of 600 nM.[22] Each value represents the mean ± SEM of three independent experiments. Dunnett's multiple comparison test was performed using GraphPad Prism software (**: $p < 0.01$, DMSO as control).[29]

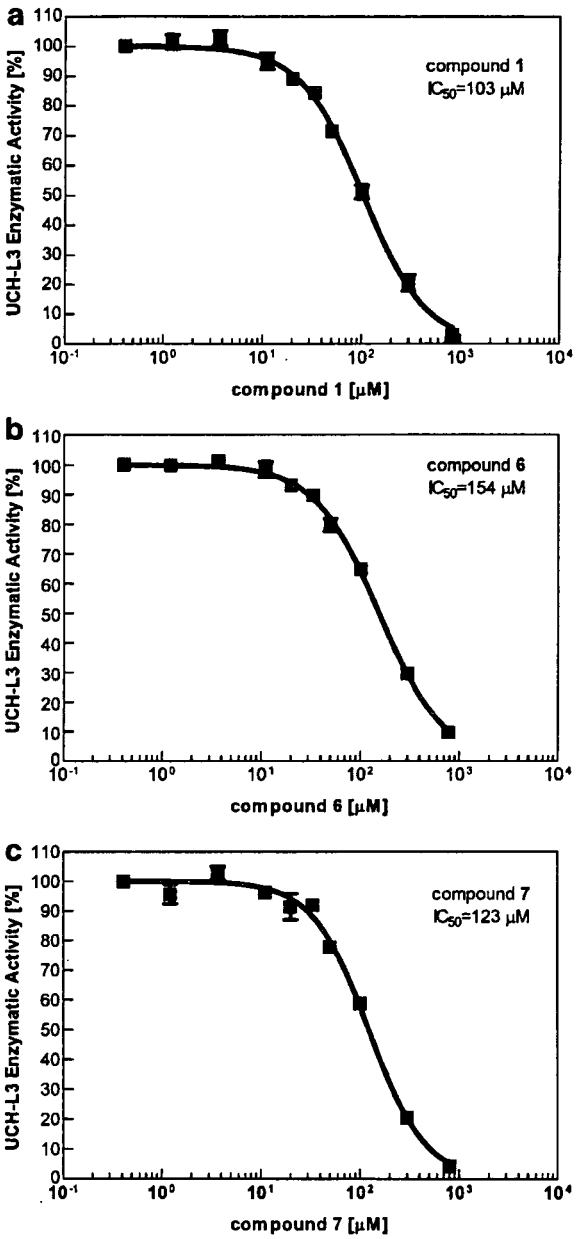

Figure 3. IC_{50} curves of compounds for UCH-L3 enzymatic activity. (a) Compound **1**, (b) compound **6**, and (c) compound **7**. The horizontal axis shows the concentration of each compound. The vertical axis shows the relative UCH-L3 enzymatic activity [%] in comparison with maximal initial velocity. IC_{50} values are shown in graphs. Each plotted value represents the mean ± SEM of three independent experiments.

In order to show that the compounds **1**, **6**, and **7** bind to UCH-L3, Biacore 100 analysis was conducted. Biacore 100 analysis detects interaction between a small molecule and protein and enables quantification of the interaction.[23] The results showed that binding of each compound to UCH-L3 increased and was dependent on the concentration of the compound **6** (data not shown).

2.5. Predicted binding mode

Figure 5 shows the predicted binding modes of compounds **1**, **6**, and **7** to UCH-L3. Since chemical formulae of the three compounds are similar to each other, the predicted docked structures of these and UCH-L3 have similar binding modes. Two hydrogen bonds were observed between the docked ligand and two amino acid residues in the predicted compound **1**/UCH-L3 complex structure; the carbonyl group of compound **1** appears to form a hydrogen bond to the NH group of Ala11, and the pyrrole C=O appears to form a hydrogen bond to the hydroxyl group of Thr157. Three hydrogen bonds were predicted between the docked ligand and two amino acid residues in the compound **6**/UCH-L3 complex structure; the thiadiazole group of compound **6** appears to form a hydrogen bond to the NH group of Leu9, and

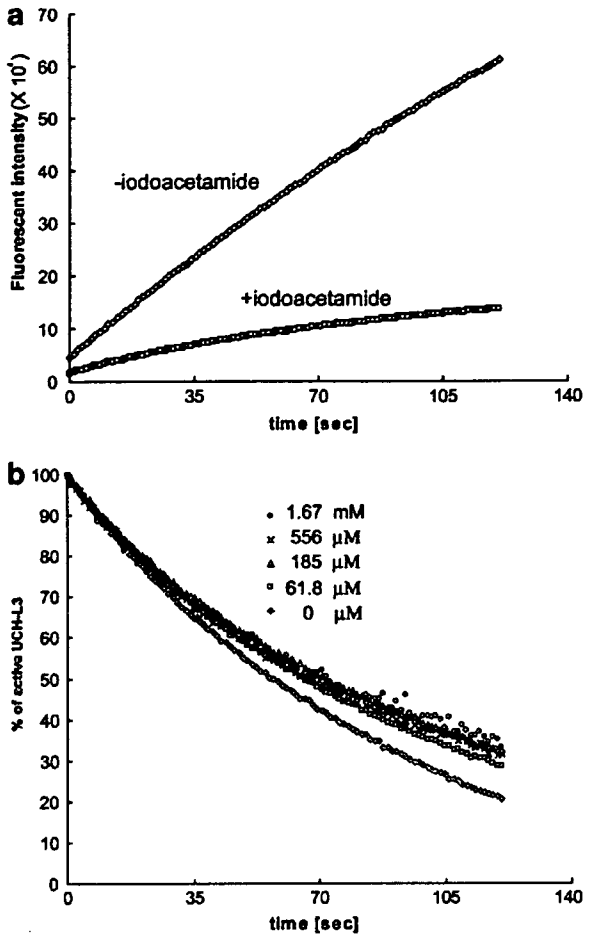

Figure 4. Competitive inhibition of compound 1. (a) Kinetics of UCH-L3-catalyzed hydrolysis of Ub-AMC with or without iodoacetamide (108 mM). (b) Reaction progress curves normalized by final fluorescence intensity representing the ratio of active UCH-L3 (for calculations, see Section 4.9), in the presence of iodoacetamide (108 mM) and compound 1 (0 μM, 61.8 μM, 185 μM, 556 μM, and 1.67 mM).

the pyrrole hydroxyl group and pyrrole C=O appear to form a hydrogen bond to the NH group of Ala11. A hydrogen bond was observed between the docked ligand and the amino acid residues of UCH-L3 in the predicted compound **7**/UCH-L3 complex structure; the carbonyl group of compound **7** appears to form a hydrogen bond to the NH group of Ala11. The predicted binding mode of compound **10**, as a non-binder, was analyzed. Four hydrogen bonds were observed between the docked ligand and the amino acid residues of UCH-L3 in the predicted compound **10**/UCH-L3 complex structure. The triazol group of compound **10** appears to form two hydrogen bonds to the hydroxyl group of Thr157, and the amino group of compound **10** appears to form a hydrogen bond to the CO group of Glu154, and to the CO group of Ser151. Although hydrogen bonds between actual inhibitors (compounds **1**, **6**, and **7**) and Ala11 were observed, compound **10**, a non-inhibitor, does not appear to form a hydrogen bond to Ala11. This hydrogen bond might be important for compounds to bind stably to the UCH-L3 active site.

2.6. Discussion; analysis of active compounds

By three-step virtual screening (DOCK, high-speed GOLD, and low-speed GOLD) of 32,799 chemicals, we identified 10 candidate chemicals that potentially inhibit UCH-L3 hydrolysis activity. We examined the actual inhibitory effects of the compounds on UCH-L3 hydrolysis activity by biochemical enzymatic assay and identified three compounds (compounds **1**, **6**, and **7**) as UCH-L3 inhibitors, with IC_{50} values of 100–150 μM. By comparing the structural formulae of the three compounds, we found that the 1,5-dihydro-2*H*-pyrrol-2-one group is likely to be important for inhibition of UCH-L3-hydrolysis activity (Fig. 6). Several common structural features can be drawn from these three chemicals (Fig. 6). First, the heteroaromatic pyrrole group is common to all three compounds. Second, each of the three compounds also contains pyridines and furoyls as heteroaromatic functional groups. Third, a carbon–oxygen double bond at position 2, a hydroxyl group at position 3, a carbonyl group at position 4, and a hydrogen atom at position 5 of the pyrrole ring are common to each compound. Fourth, a five- or six-membered cyclic group at positions 1, 4, and 5 is common to all three chemicals (Fig. 6). Furthermore, compounds **1** and **7** have two heteroaromatic groups: a pyridinyl group and a furoyl group.

The structural similarities of UCH-L3-binding chemicals have an influence on binding mode similarities. There are two main pockets in the substrate-binding site of UCH-L3: the first pocket (Pocket 1) is formed by Pro8, Glu10, and Thr157 and the second pocket (Pocket 2), the active site pocket, is formed by Asp167, Leu168, and Cys90. Docked orientations of compounds **1** and **7** are very similar, as positions 1 and 5 six-membered cyclic groups fit into each pocket. This suggests that two features among these similarities are likely to be important for stable binding to the active site: a pyrrole ring and two heteroaromatic groups, which fit into both pockets around the UCH-L3 substrate-binding site. The shape of Pocket 1 is different from that of UCH-L1,[24] another isoform of the UCH family (52% amino acid sequence identity).[25] Thus, modification of the chemical groups in Pocket 1 might be effective during drug design, to enhance specificity for UCH-L3 over UCH-L1.

Several lines of evidence indicate that UCH-L3 is associated with tumorigenesis and carcinogenesis. High-level expression and activity of UCH-L3 has been reported in multiple types of cancer cells. Expression of UCH-L3 mRNA is upregulated in breast tumors and UCH-L3 mRNA levels are associated with the histological grading of such tumors.[5] Moreover, it has been suggested that the activity of UCH-L3 is also upregulated in the majority of cervical carcinoma tissues, compared with adjacent normal tissues.[6] On the other hand, loss of UCH-L3 is known to induce cell death in knock-out studies. UCH-L3 is involved in the protection of programmed cell death in germ cells and photoreceptor cells in vivo.[7,8] Thus, the structural information of the

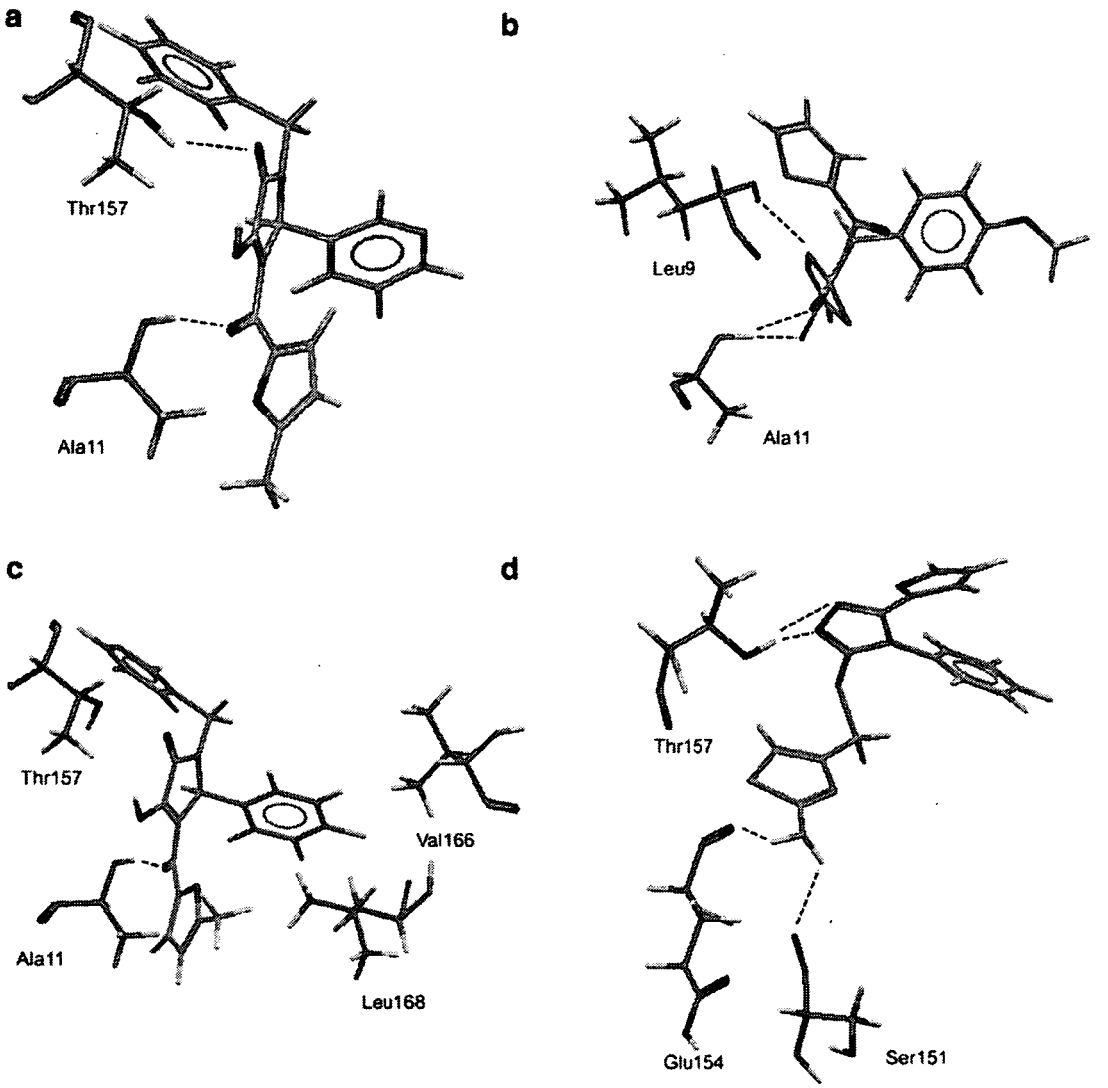

Figure 5. Illustration showing the molecular docking results. Docked orientation of (a) compound **1**, (b) compound **6**, (c) compound **7**, and (d) compound **10** in the UCH-L3 active site using GOLD and shown with interacting residues. Hydrogen bonds are shown by a dashed line. Oxygen atoms are shown in red, nitrogen atoms in blue, sulfur atoms in orange, fluorine atoms in yellow, and hydrogen atoms in gray. The enzyme carbons are shown in dark gray and those of the ligands in green.

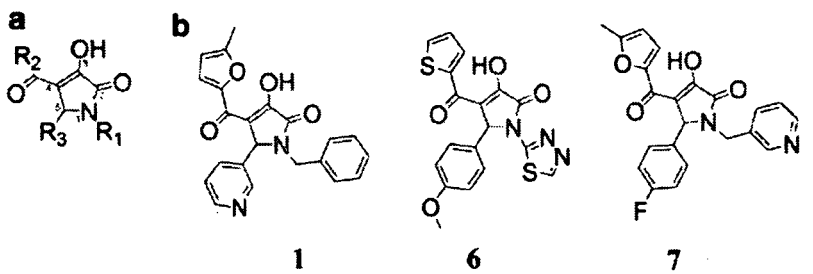

Figure 6. Structural similarities of the three compounds. (a) 1,5-Dihydro-2*H*-pyrrol-2-one group, the common basic skeleton, is shown in red. Position numbers of the pyrrole ring are shown as small characters. R_1–R_3 represent each functional group at positions 1, 4, and 5 of the pyrrole ring, respectively. (b) Structures of identified inhibitors: compounds **1**, **6**, and **7**.

UCH-L3 inhibitors we identified may be useful for future apoptosis-inducing anti-cancer drug development. UCH-L3 should be an important target for modulating cell apoptosis.

3. Conclusion

In this study, we employed three-step docking (DOCK, rough GOLD, and fine GOLD) and in vitro enzyme

assay methods, and identified three UCH-L3 inhibitors with IC_{50} values of 100–150 μM. These novel inhibitors have a dihydro-pyrrole group in common.

4. Experimental

4.1. Compound library

We used the ADME/Tox (absorption, distribution, metabolism, excretion, and toxicity) filtered virtual compound library (ChemBridge CNS-Set) which includes a collection of 32,799 chemical compounds.[18] All compounds satisfy Lipinski's Rule of five.

4.2. Protein preparation

Human UCH-L3 and ubiquitin vinylmethylester (Ub-VME) complex crystal structure data (PDB code; 1XD3) were obtained from Protein Data Bank (PDB).[17] Hydrogens were added to UCH-L3-ubiquitin complex using CVFF99 force field by Biopolymer module in Insight II 2000 suite (Accelrys, Inc., San Diego, CA). Energy was minimized by the Discover 3 module of the same suite with all heavy atoms restrained, except hydrogen, to relieve any short contacts. To use the UCH-L3 protein structure in the following docking simulations, the structures of UCH-L3 and Ub-VME complex were divided into their components.

4.3. Virtual screening

Virtual screening experiments were performed by UCSF DOCK 5.4.0[10] and GOLD 3.0.1 (CCDC, Cambridge, UK).[26] In the first screening by DOCK, the substrate-binding site was defined, by selecting ligand atom accessible spheres and describing molecular surfaces with the SPHERE_GENERATOR program in the DOCK suite. All spheres within 6 Å of root mean square deviation (RMSD) from every atom of the three C-terminal residues of energy-minimized ubiquitin were selected by the SPHERE_SELECTOR program in DOCK suite. A scoring function ($E_{int} = E_{vdw} + E_{elec}$) was used to estimate potential binding affinity. Following the first screening with rigid ligand conditions, 1780 compounds with binding energy scores of less than −30 kcal/mol were selected for a second screening by GOLD.

Using GOLD, the 1780 compounds were screened with 7–8 times speed-up settings; that is, the pre-defined genetic algorithm (GA) parameter settings to achieve calculation speed-up. The top-ranked 100 compounds were determined, then screened by default settings; the GA parameter settings for a slower calculation with greater ligand flexibility, but with a more accurate prediction. Ligand flexibility was turned on in both the 7–8 times speed-up settings and the default settings. Protein side chain flexibility was not turned on in any settings. The virtual tripeptide structure composed of three C-terminal residues of the energy-minimized ubiquitin was set as the reference ligand to define the ligand-binding site. All protein atoms within 5 Å of each ligand atom were used for defining the binding site. The solvent-accessible surfaces of the docking region were restricted by a cavity detection algorithm.[27] As a result, the binding site was composed of 174 active atoms (automatically selected by GOLD software). A method for defining the binding site with tripeptide yielded the best score among other methods using shorter or longer C-terminal peptide sequences of ubiquitin (data not shown). Ten docking solutions for each docked molecule were scored and the top three were saved for post-screening evaluations. Potential hydrogen bonds and van der Waals contacts were identified using Silver 1.0 (CCDC, Cambridge, UK).[28] Ligands predicted to be tight-binders by both DOCK and GOLD were applied to further in vitro experimental validation. All calculations were performed on seven Linux or Cygwin 2–3 GHz/Pentium IV CPU personal computers.

4.4. Statistical analysis

All statistical analysis was performed by GraphPad Prism 4 (GraphPad Software, Inc., San Diego, CA).[29]

4.5. Reagents

Human recombinant UCH-L3, ubiquitin-7-amido-4-methylcoumarin (Ub-AMC), and ubiquitin-aldehyde (Ub-H) were purchased from Boston Biochem, Inc. (Cambridge, MA). 4,5,6,7-Tetrachloroindan-1,3-dione (TCI) was purchased from Fisher Scientific International Inc. (Hampton, NH). Iodoacetamide was purchased from Sigma–Aldrich Corporation (St. Louis, MO). Compounds within ChemBridge CNS-Set (Supplier IDs given in parentheses) are as follows: compound **1**: 1-benzyl-3-hydroxy-4-(5-methyl-2-furoyl)-5-(3-pyridinyl)-1,5-dihydro-2*H*-pyrrol-2-one (7504601); compound **2**: 3-[4-methyl-5-({[3-(2-thienyl)-1,2,4-oxadiazol-5-yl]methyl}thio)-4*H*-1, 2,4-triazol-3-yl]-1*H*-indole (7950509); compound **3**: *N*-{4-[1-(2-furoyl)-5-(2-furyl)-4,5-dihydro-1*H*-pyrazol-3-yl]phenyl}methanesulfonamide (7977303); compound **4**: N^1-cyclopropyl-N^2-(4-methoxyphenyl)-N^2-[(4- methylphenyl)sulfonyl]glycinamide (6382507); compound **5**: *N*-{3-[1-acetyl-5-(2-thienyl)-4,5-dihydro-1*H*-pyrazol-3-yl]phenyl}ethanesulfonamide (7909542); compound **6**: 3-hydroxy-5-(4-methoxyphenyl)-1-(1,3,4-thiadiazol-2-yl)-4-(2-thienylcarbonyl)-1,5-dihydro-2*H*-pyrrol-2-one (6237842); compound **7**: 5-(4-fluorophenyl)-3-hydroxy-4-(5-methyl-2-furoyl)-1-(3-pyridinylmethyl)-1,5-dihydro-2*H*-pyrrol-2-one (6771097); compound **8**: N^1-cyclopropyl-N^2-[(4-methoxyphenyl)sulfonyl]-N^2-(4-methylphenyl)glycinamide (6699002); compound **9**: N^1-cyclopentyl-N^2-(3-methoxyphenyl)-N^2-(phenylsulfonyl)glycinamide (6187162); and compound **10**: 4-({[5-(2-furyl)-4-phenyl-4*H*-1,2,4-triazol-3-yl]thio}methyl)-1,3-thiazol-2-amine (9012750) were purchased from ChemBridge Corporation (San Diego, CA).

4.6. Enzymatic assay

UCH-L3 activity was assayed using modification of a technique described in previous studies.[22,30] The enzyme

reactions were carried out at a final volume of 205 μl on Costar 96-well black assay plates (part number 3915, Corning Inc., Corning, NY). Then, 5 μl of solution containing each compound (100% DMSO), or 5 μl of 100% DMSO as a negative control, was added to 100 μl of enzyme buffer solution (50 pM of UCH-L3, 20 mM Hepes [pH 7.8], 0.5 mM EDTA, 5 mM dithiothreitol [DTT], and 0.1 mg/ml ovalbumin) in each well. The solution was incubated for 30 min at room temperature. To start the enzyme reaction, 100 μl of substrate buffer solution (82 nM of ubiquitin-AMC, 20 mM Hepes [pH 7.8], 0.5 mM EDTA, 5 mM DTT, and 0.1 mg/ml ovalbumin) was added to each well. AMC fluorescence (excitation wavelength: 355 nm, emission wavelength: 460 nm) was subsequently measured 40 times every 3 s with a Wallac 1420 multi-label counter (Perkin-Elmer, Wellesley, MA).

4.7. K_m determination

Fifty microliters of enzyme buffer solution was added to each plate well. The solution was incubated for 30 min at room temperature. To start the enzyme reaction, 50 μl of substrate buffer solution (23.1, 46.3, 92.5, 185, 370, and 740 nM of ubiquitin-AMC; the concentrations of other components were as described previously) was added to each well. Fluorescence of AMC was measured 40 times every 3 s with the Wallac multi-label counter. Initial velocities (from 0 to 30 s) were used for K_m determination, using GraphPad Prism 4 software.[29]

4.8. Experimental IC_{50} determination

Five microliters of solution containing each compound (0.412 μM, 1.23, 3.70, 11.1, 20, 33.3, 50, 100, 300, and 700–850 μM) or 5 μl of 100% DMSO (as a negative control) diluted in 100 μl of enzyme buffer solution was added to each plate well. This solution was incubated for 30 min at room temperature. To start the enzyme reaction, 100 μl of substrate buffer solution was added to each well. Fluorescence of AMC was measured 40 times every 3 s with the Wallac multi-label counter. Initial velocities (from 0 to 30 s) were used for IC_{50} determination, using GraphPad Prism 4 software.[29]

4.9. Active site binding experiment

Modification of a technique described in previous studies was used to determine whether or not the compounds bind to the active site.[22] Five microliters of solution containing compound **1** (0 μM, 61.8 μM, 185 μM, 556 μM, and 1.67 mM) or 5 μl of 100% DMSO (as a negative control) diluted in 80 μl of enzyme buffer solution (UCH-L3: 1 nM) was added to each plate well. This solution was incubated for 30 min at room temperature. To start the enzyme reaction, 80 μl of substrate buffer solution (Ub-AMC: 1 μM) was added to each well, followed within 2 s by addition of 40 μl of iodoacetamide (108 mM) or water as a negative control. Fluorescence of AMC was measured 100 times every second using the Wallac multi-label counter. The percentage of active site survival $[(F_{saturated} - F_t)/(F_{saturated} - F_{t=0}) \times 100]$ was calculated.

Acknowledgments

This work was supported by Grants-in-Aid for Scientific Research from the Ministry of Health, Labour and Welfare of Japan, Grants-in-Aid for Scientific Research from the Ministry of Education, Culture, Sports, Science and Technology of Japan, a grant from the Program for Promotion of Fundamental Studies in Health Sciences of the National Institute of Biomedical Innovation, a grant from Japan Science and Technology Cooperation, and a grant from New Energy and Industrial Technology Development Organization. We thank Takashi Kaburagi for demonstrating how to set up the DOCK software.

References and notes

1. Ciechanover, A.; Schwartz, A. L. *Proc. Natl. Acad. Sci. U.S.A.* **1998**, *95*, 2727–2730.
2. Pickart, C. M.; Rose, I. A. *J. Biol. Chem.* **1985**, *260*, 7903–7910.
3. Waldmeier, P.; Bozyczko-Coyne, D.; Williams, M.; Vaught, J. L. *Biochem. Pharmacol.* **2006**, *72*, 1197–1206.
4. Aktas, O.; Waiczies, S.; Zipp, F. *J. Neuroimmunol.* **2007**, *184*, 17–26.
5. Miyoshi, Y.; Nakayama, S.; Torikoshi, Y.; Tanaka, S.; Ishihara, H.; Taguchi, T.; Tamaki, Y.; Noguchi, S. *Cancer Sci.* **2006**, *97*, 523–529.
6. Rolen, U.; Kobzeva, V.; Gasparjan, N.; Ovaa, H.; Winberg, G.; Kisseljov, F.; Masucci, M. G. *Mol. Carcinog.* **2006**, *45*, 260–269.
7. Kwon, J.; Wang, Y. L.; Setsuie, R.; Sekiguchi, S.; Sato, Y.; Sakurai, M.; Noda, M.; Aoki, S.; Yoshikawa, Y.; Wada, K. *Am. J. Pathol.* **2004**, *165*, 1367–1374.
8. Sano, Y.; Furuta, A.; Setsuie, R.; Kikuchi, H.; Wang, Y. L.; Sakurai, M.; Kwon, J.; Noda, M.; Wada, K. *Am. J. Pathol.* **2006**, *169*, 132–141.
9. Kuntz, I. D.; Blaney, J. M.; Oatley, S. J.; Langridge, R.; Ferrin, T. E. *J. Mol. Biol.* **1982**, *161*, 269–288.
10. Ewing, T. J.; Makino, S.; Skillman, A. G.; Kuntz, I. D. *J. Comput. Aided Mol. Des.* **2001**, *15*, 411–428.
11. FlexX, BioSolveIT GmbH, Sankt Augustin, Germany, <http://www.biosolveit.de/>.
12. Peng, H.; Huang, N.; Qi, J.; Xie, P.; Xu, C.; Wang, J.; Yang, C. *Bioorg. Med. Chem. Lett.* **2003**, *13*, 3693–3699.
13. McNally, V. A.; Gbaj, A.; Douglas, K. T.; Stratford, I. J.; Jaffar, M.; Freeman, S.; Bryce, R. A. *Bioorg. Med. Chem. Lett.* **2003**, *13*, 3705–3709.
14. Olsen, L.; Jost, S.; Adolph, H. W.; Pettersson, I.; Hemmingsen, L.; Jorgensen, F. S. *Bioorg. Med. Chem.* **2006**, *14*, 2627–2635.
15. Miteva, M. A.; Lee, W. H.; Montes, M. O.; Villoutreix, B. O. *J. Med. Chem.* **2005**, *48*, 6012–6022.
16. Johnston, S. C.; Larsen, C. N.; Cook, W. J.; Wilkinson, K. D.; Hill, C. P. *EMBO J.* **1997**, *16*, 3787–3796.
17. Misaghi, S.; Galardy, P. J.; Meester, W. J.; Ovaa, H.; Ploegh, H. L.; Gaudet, R. *J. Biol. Chem.* **2005**, *280*, 1512–1520.
18. RPBS, Paris, France, <http://bioserv.rpbs.jussieu.fr/RPBS/cgi-bin/Ressource.cgi?chzn_lg=an&chzn_rsrc=Collections/>.
19. GOLD User Guide, 16.2.1, CCDC, Cambridge, UK, <http://www.ccdc.cam.ac.uk/support/documentation/gold/3_1/gold31.pdf/>.
20. Dang, L. C.; Melandri, F. D.; Stein, R. L. *Biochemistry* **1998**, *37*, 1868–1879.

21. Mason, D. E.; Ek, J.; Peters, E. C.; Harris, J. L. *Biochemistry* **2004**, *43*, 6535–6544.
22. Liu, Y.; Lashuel, H. A.; Choi, S.; Xing, X.; Case, A.; Ni, J.; Yeh, L. A.; Cuny, G. D.; Stein, R. L.; Lansbury, P. T., Jr. *Chem. Biol.* **2003**, *10*, 837–846.
23. Stenlund, P.; Frostell-Karlsson, A.; Karlsson, O. P. *Anal. Biochem.* **2006**, *353*, 217–225.
24. Das, C.; Hoang, Q. Q.; Kreinbring, C. A.; Luchansky, S. J.; Meray, R. K.; Ray, S. S.; Lansbury, P. T.; Ringe, D.; Petsko, G. A. *Proc. Natl. Acad. Sci. U.S.A.* **2006**, *103*, 4675–4680.
25. Kurihara, L. J.; Semenova, E.; Levorse, J. M.; Tilghman, S. M. *Mol. Cell. Biol.* **2000**, *20*, 2498–2504.
26. Jones, G.; Willett, P.; Glen, R. C.; Leach, A. R.; Taylor, R. *J. Mol. Biol.* **1997**, *267*, 727–748.
27. Hendlich, M.; Rippmann, F.; Barnickel, G. *J. Mol. Graph. Model.* **1997**, *15*, 359–363.
28. Silver, CCDC, Cambridge, UK, <http://www.ccdc.cam.ac.uk/>.
29. GraphPad Prism 4, GraphPad Software, San Diego, CA, <http://www.graphpad.com/www/about.htm/>.
30. Nishikawa, K.; Li, H.; Kawamura, R.; Osaka, H.; Wang, Y. L.; Hara, Y.; Hirokawa, T.; Manago, Y.; Amano, T.; Noda, M.; Aoki, S.; Wada, K. *Biochem. Biophys. Res. Commun.* **2003**, *304*, 176–183.

Available online at www.sciencedirect.com
ScienceDirect
European Journal of Pharmacology 573 (2007) 20–28
www.elsevier.com/locate/ejphar

Alpha 1-adrenoceptor agonists protect against stress-induced death of neural progenitor cells

Hiroki Ohashi [a,b], Kaori Nishikawa [a,c], Koichi Ayukawa [a,d], Yoko Hara [a], Mika Nishimoto [a,e], Yoshihisa Kudo [e], Toshiaki Abe [b], Shunsuke Aoki [a,c,f,*], Keiji Wada [a,f]

[a] *Department of Degenerative Neurological Diseases, National Institute of Neuroscience, NCNP, Kodaira, Tokyo 187-8502, Japan*
[b] *Department of Neurosurgery, Jikei University Graduate School of Medicine, Minatoku, Tokyo 105-8401, Japan*
[c] *NEDO (New Energy and Industrial Technology Development Organization), Kawasaki, Kanagawa 212-8554, Japan*
[d] *Japan Society for the Promotion of Science (JSPS), Chiyodaku, Tokyo 102-8471, Japan*
[e] *Laboratory of Cellular Neurobiology, Tokyo University of Pharmacy and Life Science, Hachioji, Tokyo 192-0392, Japan*
[f] *CREST (Core Research for Evolutional Science and Technology) of Japan Science and Technology Corporation (JST), Kawaguchi, Saitama 332-0012, Japan*

Received 15 February 2007; received in revised form 18 June 2007; accepted 26 June 2007
Available online 12 July 2007

Abstract

Here, we show that α_1-adrenoceptor agonists suppress stress-induced death of mouse embryonic brain-derived neural progenitor cells (NPCs). NPCs highly expressed both α_{1A}- and α_{1B}-adrenoceptor genes, whereas the gene encoding α_{1D}-adrenoceptor was expressed at low levels. Application of the α_1-adrenoceptor agonists phenylephrine and cirazoline significantly promoted cell survival of embryonic NPCs that had been exposed to stress, as measured by a lactate dehydrogenase release assay, but had no remarkable effect on differentiation of the NPCs. Both phenylephrine and cirazoline protected NPCs from death induced by growth factor deprivation, N2 nutrient deprivation, tunicamycin treatment or staurosporine treatment. Phenylephrine and cirazoline treatments both maximally reduced stress-induced cell death by ~60% but did not change the percentage of undifferentiated cells as measured by nestin staining. Moreover, phenylephrine and cirazoline treatments did not affect the cellular activities of caspase-3 and caspase-7 but markedly reduced propidium iodide penetration into the cytoplasm, suggesting that α_1-adrenoceptor agonists inhibit caspase-3/7-independent death of the embryonic NPCs.

Keywords: α_1-adrenoceptor; GPCR; Neural progenitor cell; Cell death; Cell stress; Phenylephrine; Cirazoline

1. Introduction

The noradrenergic system is proposed to play multiple roles in the adult central nervous system (CNS). Apart from its classical transmitter signaling action, noradrenaline has important roles in attention, arousal, and memory reviewed in Murchison et al., (2004); Southwick et al., (1999). Furthermore, it was proposed that noradrenaline influences the survival, maintenance and plasticity of CNS neurons, including the regulation of endogenous neurotrophin systems, glial function, CNS energy utilization and extracellular homeostasis, and has anti-inflammatory and anti-oxidant effects reviewed in Marien et al., (2004). All cell surface adrenoceptors are members of the G protein-coupled receptor family and mediate responses to extracellular noradrenaline. To date, three subfamilies of adrenoceptors (α_1, α_2 and β) have been identified (Bylund et al., 1995). The adrenoceptors are expressed in many tissues, particularly in the cardiovascular, genitourinary and nervous systems. High levels of adrenoceptors are also present in the neocortex during embryogenesis (Lidow and Rakic, 1992), and there are regional concentrations of α_1, α_2, and β adrenoceptors in the fetal forebrain (Lidow and Rakic, 1994). There are three subtypes of α_1-adrenoceptors, the α_{1A}, α_{1B}, α_{1D}-adrenoceptor, with varying degrees of efficiency of G protein (Gq/11) coupling ($\alpha_{1A}>\alpha_{1B}>\alpha_{1D}$ adrenoceptor) reviewed in Hieble et al., (1995). This leads to activation of downstream signal

* Corresponding author. Department of Degenerative Neurological Diseases, National Institute of Neuroscience, National Center of Neurology and Psychiatry, 4-1-1 Ogawahigashi, Kodaira, Tokyo 187-8502, Japan. Tel.: +81 42 346 1715; fax: +81 42 346 1745.
E-mail address: aokis@ncnp.go.jp (S. Aoki).

0014-2999/$ - see front matter © 2007 Elsevier B.V. All rights reserved.
doi:10.1016/j.ejphar.2007.06.060

transduction pathways, including Ca^{2+}, arachidonic acid, phospholipase C and phospholipase D signals reviewed in Zhong and Minneman (1999). α_1-adrenoceptors are specifically localized to NPCs located in the ventricular zone and subventricular zone in the embryonic rat forebrain, and noradrenaline-containing fibers are also present in both the ventricular zone and subventricular zone (Pabbathi et al., 1997). In addition, noradrenaline has been suggested to regulate development of the murine forebrain. The β-adrenoceptor agonist isoproterenol alters proliferation and differentiation of neural precursors in the cerebral cortex (Slotkin et al., 1988). α_1-adrenoceptors were also implicated in controlling cell proliferation and survival in a rat cortical mixed cell culture and in a heterochronic coculture system of the rat neocortex and rostral pons (Pabbathi et al., 1997; Popovik and Haynes, 2000). Although the functions of α_1-adrenoceptors in the mixed-culture NPCs and in the organ culture were investigated, the function of α_1-adrenoceptors and the direct effects of α_1-adrenoceptor-selective agonists such as phenylephrine and cirazoline in isolated pure embryonic NPCs are not known.

The precise role of the α_1-adrenoceptor-mediated signal in embryonic cortical NPCs remains obscure, because the effects observed in the mixed-cell and organ culture experiments possibly reflect the secondary and tertiary effects mediated by multiple cellular interactions (glial cell-progenitor, neuronal cell-progenitor and neuronal cell-glial cell-progenitor interactions). As such, the aim of this study is to know the primary biological effect of α_1-adrenoceptor activation in the NPCs. We addressed the biological effects of α_1-adrenoceptor-selective agonists on highly purified embryonic NPCs. Our data indicate that these agonists inhibit death of NPCs cultured under various stress conditions but do not affect proliferation, differentiation or caspase-3/7-activity.

2. Materials and methods

2.1. Animals

Pregnant C57BL/6J mice were purchased from CLEA Japan (Tokyo, Japan). Animal care and handling were in accordance with institutional regulations for animal care and public law, and were approved by the Animal Investigation Committee of the National Institute of Neuroscience, Japan.

2.2. Antibodies and reagents

Monoclonal and polyclonal antibodies used in this study were as follows: monoclonal anti-nestin (Becton Dickinson, Lexington, KY), monoclonal anti-tuj1 (Covance, Berkeley, CA), polyclonal anti-glial fibrillary acidic protein (Dako, Carpinteria, CA), monoclonal anti-galactocerebroside (Chemicon International, Temecula, CA). The secondary antibodies conjugated to Alexa Fluor dye were purchased from Molecular Probes (Eugene, OR). α_1-adrenoceptor agonists used in this study were (*R*)-3-[1-hydroxy-2-(methylamino) ethyl] phenol (phenylephrine; Sigma, St. Louis, MO) and 2-[(2-cyclopropyl-phenoxy) methyl]-4, 5-dihydro-1H-imidazole (cirazoline; Tocris, Ellisville, MO). Each agonist was dissolved in Neurobasal™ medium (Invitrogen, Carlsbad, CA). Staurosporine and tunicamycin (Sigma) were dissolved in dimethyl sulfoxide (DMSO). Each solution was added to the medium, and the final concentration of DMSO in the medium was adjusted to at most 0.1% (v/v). Medium containing the same amount of organic solvent was used as a negative control.

2.3. Cortical NPCs culture

Cortical NPCs were cultured as previously described (Fukazawa et al., 2006). Briefly, embryos were removed from pregnant C57BL/6J mice and were staged according to morphological criteria to confirm gestational age. Developing mouse brain and cerebral cortex containing the ventricular and subventricular zones were dissected from embryonic day 14 (E14) embryos. Cells were mechanically dissociated by trituration and plated at 3.0×10^6 cells per 10-cm dish (BD) precoated with 15 μg/ml poly-L-ornithine (Sigma) and 1 μg/ml fibronectin (Nitta Gelatin, Osaka, Japan). Cells were expanded for 4 days in serum-free Neurobasal medium supplemented with 0.5 mM L-glutamine (Invitrogen), 100 U/ml penicillin, 100 μg/ml streptomycin (Invitrogen) and B27 (biotin, L-carnitine, corticosterone, ethanolamine, D(+)-galactose, glutathione (reduced), linoleic acid, linolenic acid, progesterone, putrescine, retinyl acetate, selenium, T3 (triodo-l-thyronine), DL-α-tocopherol (vitamin E), DL-α-tocopherol acetate, bovine serum albumin, catalase, insulin, superoxide dismutase, transferrin, vitamin A (Brewer et al., 1993); Invitrogen). N2 supplement (100 mg/l apo-transferrin, 5 mg/l insulin, 16 mg/l putrescine, 6.3 μg/l progesterone, 5 μg/l selenite; Sigma) were used for stress experiments instead of the B27 supplement. This medium was supplemented with 10 ng/ml basic fibroblast growth factor (bFGF; PeproTech, Rocky Hill, NJ) except when mentioned otherwise. Cultures were maintained at 37 °C in an atmosphere of 95% air and 5% CO_2. For secondary cultures, bFGF-expanded cortical NPCs were washed in warm Hanks' balanced salt solution, detached with mechanically pipetting, and resuspended in Neurobasal medium. Cells were then re-seeded on 24-well plates (Nunc; 1.8×10^5 cells/well), or 48-well plates (Nunc; 1.5×10^5 cells/well) precoated with poly-L-ornithine and fibronectin.

2.4. Real-time quantitative reverse-transcription (RT)-PCR

Real-time quantitative RT-PCR with the SYBR Green-based detection method was performed as previously described (Aoki et al., 2002). Total RNA was isolated from cultured cortical NPCs and E14 mouse cerebral cortex. These RNAs (1 μg) were treated with DNase I and converted to cDNA with Superscript II reverse transcriptase (Invitrogen) and random hexamer primers according to the manufacturer's instructions. The efficiency of reverse transcription and the quality of cDNA was compared with the efficiency of PCR amplification of the hypoxanthine guanine phosphoribosyl transferase (hprt) gene (GenBank accession ID. NM_013556; forward primer, 5′-TCTTTGCTGACCTGCTGGATT-3′; reverse primer, 5′-TATGTCCCCCGTTGACTGATC-

3′). Primers were designed for the α_{1A} (NM_013461), α_{1B} (NM_007416) and α_{1D} (NM_013460) adrenoceptor genes using Primer Express software (Perkin-Elmer, Torrance, CA). The forward and reverse primer sequences were as follows: 5′-TTTCAAGCCACCGGAAACA-3′ and 5′-ACTGGATTCGCAGCACATTCT-3′ (α_{1A}); 5′-AACCCTTCTACGCCCTCTTTTC-3′ and 5′-CCAGATTCTTGGTGGTCCTCTT-3′ (α_{1B}); and 5′-TCGCTCAAGTATCCAGCCATT-3′ and 5′-AACCTAGTAGCGGTCCCACAGA-3′ (α_{1D}). SYBR Green-based real-time RT-PCR was performed in 12.5-μl reactions (ABI PRISM 7700 Sequence Detection System, Perkin-Elmer). PCR products were analyzed with agarose gel electrophoresis. We checked each primer individually to ensure that the primer was selective for the target (data not shown). We also ensured that no band was observed in gel electrophoresis of PCRs that included distilled water or total RNA preparation without reverse transcriptase as template. The quantitative RT-PCR method (User Bulletin #2, Applied Biosystems, Foster City, CA) was modified to establish an expression level index for mRNA (Aoki et al., 2002), and the SYBR Green signal for the hprt amplicon was used as a reference. Amplification efficiency was determined and confirmed in a control PCR experiment using serial cDNA dilutions as templates. The real-time RT-PCR products were analyzed using the Applied Biosystems sequence detection system software 1.7.

2.5. LDH and ATP assay

The number of non-viable cortical NPCs was quantitatively assayed by measuring the activity of the cytosolic enzyme lactate dehydrogenase (LDH) released into the culture medium after membrane rupture. LDH activity was measured using the cytotoxicity assay CytoTox-ONE™ Homogeneous Membrane Integrity Assay (Promega, Madison, WI). To quantify the number of viable cells in cultured cortical NPCs, the amount of cellular ATP was measured using the CellTiter-Glo™ Luminescent Cell Viability Assay (Promega). These assays were performed in accordance with the manufacturer's protocol and on secondary cultured cortical NPCs as described above. Four hundred μl (1.5×10^5 cells/well) of cell suspension was added to each well of a 48-well plate (Nunc) precoated with poly-L-ornithine and fibronectin. After 24 h, cells were treated without or with 10 μM phenylephrine or cirazoline with different concentrations of bFGF or under different stress conditions as described in the figure legends. Cultures were then returned to the 37 °C incubator for 24 h, and assessment of LDH release in the media and amount of ATP was conducted with a Wallac 1420 multilabel counter (Perkin-Elmer, Finland).

2.6. Immunocytochemistry

Cells were stained as we have previously described with minor modifications (Sakurai et al., 2006). Briefly, all incubations and washes were performed at room temperature. Cells were fixed with 3.8% formaldehyde in phosphate-buffered saline (PBS) for 10 min and permeabilized with 0.02% (w/v) Triton X-100 in PBS for 5 min. Fixed cells were blocked with 3.3% goat serum in PBS for 30 min. Cells were incubated for 30 min with anti-nestin (neural progenitor marker; 1:500), anti-tuj1 (early neuronal cell marker; 1:500)(Sakurai et al., 2006), anti-glial fibrillary acidic protein (astrocyte marker; 1:1000) or anti-galactocerebroside (immature oligodendrocyte marker; 1:200)(Fukazawa et al., 2006). These cells were incubated with diluted secondary antibody (1:200) conjugated to Alexa Fluor for 30 min. All primary and secondary antibodies were diluted in 1% goat serum in PBS before use. The fluorescence microscopy images were obtained with an IX70 microscope (Olympus).

2.7. Quantification of enzymatic activities of caspases

Caspase-3 and caspase-7 protease activities were determined using the Caspase-Glo™ 3/7 Assay kit (Promega). All assays were performed on secondary cultured cortical NPCs as described above. Four hundred μl (1.5×10^5 cells/well) of cell suspension was added to each well of a 48-well plate (Nunc) precoated with poly-L-ornithine and fibronectin. After 24 h, cells were treated with or without 10 μM phenylephrine in medium lacking the N2 supplement as described in the figure legends. Cultures were then returned to the 37 °C incubator for 24 h, and caspase-3 and -7 activities were assessed with a Wallac 1420 multilabel counter.

2.8. Measurement of cell death using propidium iodide

All assays were performed on secondary cultured cortical NPCs as described above. Four hundred μl (1.5×10^5 cells/well) of cell suspension was added to each well of a 48-well plate (Nunc) precoated with poly-L-ornithine and fibronectin. After 24 h, cells were treated with or without 10 μM phenylephrine in medium lacking the N2 supplement. Cultures were then returned to the 37 °C incubator and maintained for 24 h, then stained with 1 μg/ml propidium iodide. Only dead cells with permeable plasma membranes were stained with propidium iodide. Positive controls were stained with propidium iodide after fixing with 3.8% formaldehyde in PBS for 10 min and permeabilized with 0.02% Triton X-100 in PBS. Dead cells and positive controls stained with propidium iodide were counted by fluorometry (Wallac 1420 multilabel counter).

2.9. Statistical analysis

Results are expressed as the mean±standard error of the mean (S.E.M.). Either the Student's *t*-test or Dunnett's multiple range test was used to evaluate the data using Prism software version 4.03 (GraphPad, San Diego, CA). Values of $P<0.01$ and $P<0.05$ were considered statistically significant depending on the specific experiment.

3. Results

3.1. Embryonic cortical NPCs express α_1-adrenoceptor genes

We analyzed gene expression levels of the three α_1-adrenoceptors, and all were expressed both in the E14 embryonic

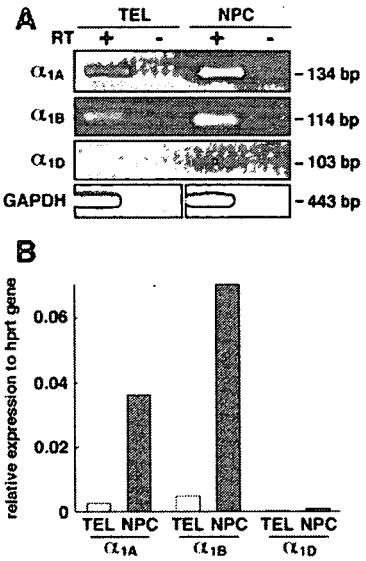

Fig. 1. NPCs derived from E14 telencephalon express α_{1A}-adrenoceptor (α_{1A}), α_{1B}-adrenoceptor (α_{1B}) and α_{1D}-adrenoceptor (α_{1D}). Total RNA isolated from cultured NPCs and E14 mouse telencephalon (TEL) was reverse-transcribed, and the resultant cDNA was used in RT-PCR analysis. (A) As indicated on the left, the PCR products corresponding to the α_{1A}, α_{1B}, and α_{1D} adrenoceptor genes and *GAPDH* were separated on a 3% agarose gel. The size of PCR products are indicated on the right. (B) Gene expression levels of the α_{1A}, α_{1B} and α_{1D} adrenoceptor were analyzed by quantitative RT-PCR, and the expression levels relative to *hprt* are presented. The results are representative of three separate experiments that yielded similar results.

telencephalon and E14 telencephalon-derived cultured NPCs (Fig. 1A). Semi-quantitative analysis of expression levels of the α_1-adrenoceptor genes (normalized to the internal control, *hprt*) showed that the isolated NPCs highly expressed α_{1A}, α_{1B} and α_{1D} adrenoceptor genes as compared with the E14 telencephalon (Fig. 1B). Among the α_1-adrenoceptor genes, the α_{1A} and α_{1B} genes were highly expressed in the cultured NPCs, whereas a low level of expression was detected for the α_{1D} gene in both the E14 telencephalon and cultured NPCs (Fig. 1B).

3.2. Effect of the α_1-adrenoceptor agonist phenylephrine on NPC differentiation

E14 telencephalon-derived NPCs have potencies to differentiate into multiple neural cell types, including neurons, astrocytes and oligodendrocytes, in the absence of bFGF (Fig. 2). The effect of phenylephrine, an α_1-adrenoceptor-selective agonist, on NPC differentiation was examined using the neural cell differentiation marker tuj1 for neuronal cells, glial fibrillary acidic protein for astroglial cells and galactocerebroside for oligodendrocytes. At 72 h after bFGF deprivation, 41.8±1.0% of the NPCs had differentiated into tuj1-positive (tuj1$^+$) cells, 40.6±6.0% of the NPCs had differentiated into glial fibrillary acidic protein-positive (GFAP$^+$) cells and 9.4±1.1% were galactocerebroside-positive (GC$^+$) (Fig. 2A and B). Phenylephrine treatment did not significantly change the percentages of neuronal and glial cells (tuj1$^+$, 38.1±3.2%; GFAP$^+$, 28.7±3.1%; and GC$^+$, 6.2±1.0%) in cultures lacking bFGF (Fig. 2A and B). These results indicate that phenylephrine did not affect NPC differentiation induced by bFGF deprivation. We also examined the effect of phenylephrine on neural differentiation of NPCs in cultures containing bFGF and again found no effect on neuronal or glial differentiation (data not shown).

3.3. α_1-adrenoceptor agonists protect NPCs from cell death

It has been reported that activation of α_1-adrenoceptors stimulates DNA synthesis of embryonic NPCs in mixed culture conditions (Pabbathi et al., 1997). Primary NPC cultures prepared from the telencephalon contain a considerable number of neuronal cells (>10%) that also express α_1-adrenoceptors (Papay et al., 2006). To determine whether the previously reported activation of DNA synthesis was indicative of NPC proliferation or proliferation by secondary effect via other cell types contaminating the culture, we re-seeded cultured NPCs from a primary culture to prepare highly purified secondary

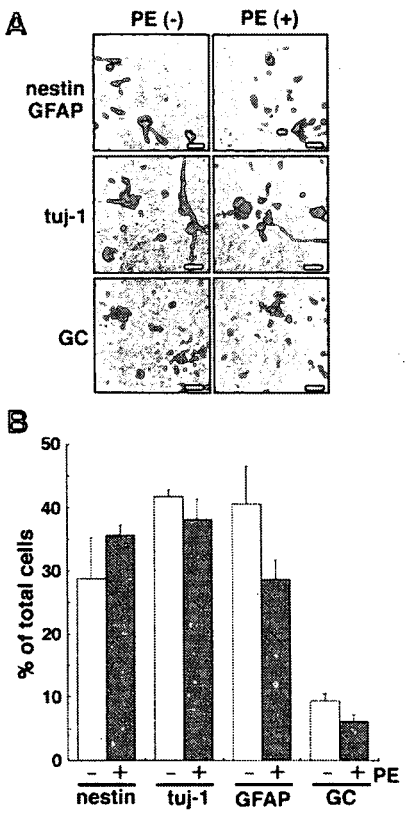

Fig. 2. Effect of the α_1-adrenoceptor agonist phenylephrine on NPC differentiation. (A) Immunofluorescence staining was carried out after 72 h on NPC cultures with or without phenylephrine. Fluorescence microscopic images of cells labeled with anti-nestin (green), anti-GFAP (red), anti-tuj1 (green) and anti-galactocerebroside (green) are shown; nuclei are stained with Hoechst (blue). Scale bar=20 μm. Similar results were obtained in two independent experiments. (B) Secondary cultured NPCs from the E14 mouse telencephalon were maintained *in vitro* for 72 h without or with 10 μM phenylephrine (PE). After 72 h, cells were fixed and immunostained for tuj1, glial fibrillary acidic protein (GFAP), nestin and galactocerebroside (GC). The number of nestin$^+$, tuj1$^+$, GFAP$^+$ and GC$^+$ cells were counted, and the percentages are presented. Nestin was used as a marker for undifferentiated NPCs. No significant differences were observed.

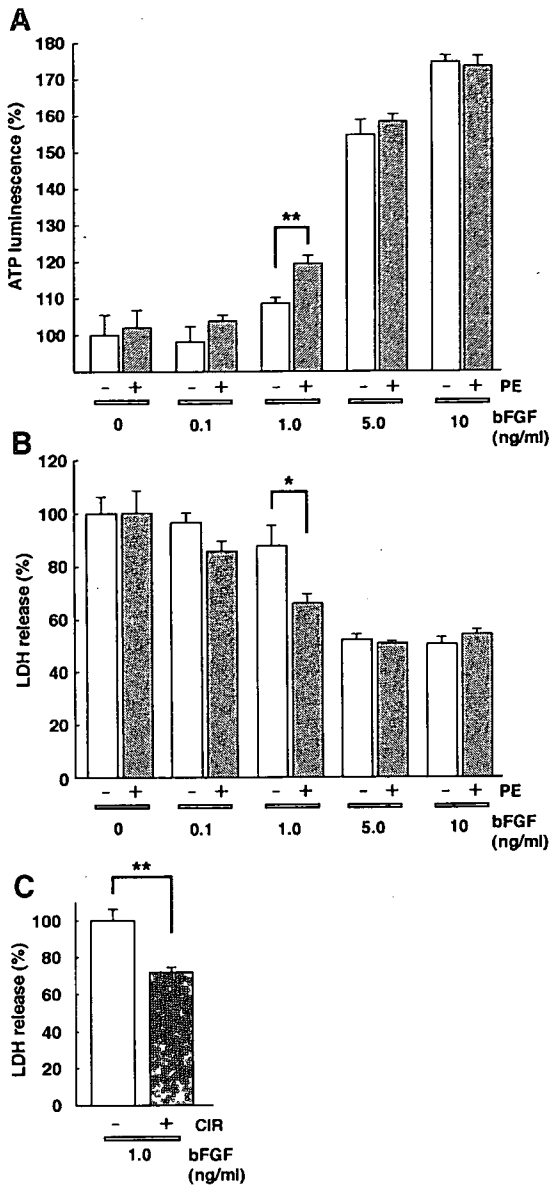

Fig. 3. Effects of α_1-adrenoceptor agonists on the number of cells and cell death of NPCs at various doses of bFGF. Secondary cultured NPCs from the E14 mouse telencephalon were treated without or with 10 μM phenylephrine at different concentrations of bFGF for 24 h. (A) The number of NPCs was examined with an ATP luminescence assay. (B) The viability of NPCs was examined with the LDH release assay. (C) Secondary cultured NPCs from the E14 mouse telencephalon were treated without or with 10 μM cirazoline in 1 ng/ml bFGF for 24 h. Cell survival was assessed by the ATP luminescence assay. Bars represent mean±S.E.M. (n=4). Significant differences are indicated by single or double asterisks (*P<0.05, **P<0.01, Student's t-test).

NPC cultures that contained over 99±0.4% nestin$^+$ undifferentiated NPCs and no more than 0.5% tuj1$^+$ neuronal cells. Using the secondary NPC culture, we examined whether phenylephrine increased the number of NPCs at various doses of bFGF (0~10 ng/ml) using an intracellular ATP luminescence assay (Crouch et al., 1993; Petty et al., 1995). We found that phenylephrine significantly increased the number of NPCs only at a moderate dose (1.0 ng/ml) of bFGF (P<0.01; Fig. 3A) and had no significant effect at high doses (5–10 ng/ml), a low dose (0.1 ng/ml) of bFGF, or no bFGF. To determine whether the effect of phenylephrine on NPCs at 1 ng/ml bFGF was due to promotion of cell growth or cell survival, we examine the effect of phenylephrine on cell death using the LDH release assay (Decker and Lohmann-Matthes, 1988), which measures destruction of the plasma membrane. Phenylephrine also significantly decreased LDH release at 1 ng/ml bFGF (P<0.05; Fig. 3B), indicating that the difference between ATP luminescence (cell numbers) of phenylephrine-treated and

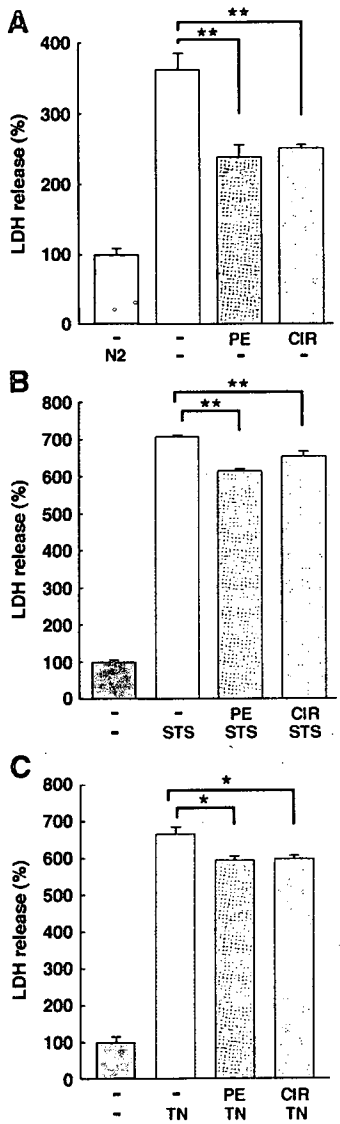

Fig. 4. Phenylephrine and cirazoline promote survival of NPCs under various stress conditions. Secondary cultured NPCs from the E14 mouse telencephalon were incubated in medium lacking N2 (A), 50 nM staurosporine (STS) (B) or 30 ng/ml tunicamycin (TN) (C) in the presence or absence of 10 μM phenylephrine (PE) or 10 μM cirazoline (CIR) for 24 h. Quantification of cell death was performed with the LDH release assay. Bars represent mean±S.E.M. (n=3~5). Significant differences are indicated by single or double asterisks (*P<0.05, **P<0.01, Dunnett's test).

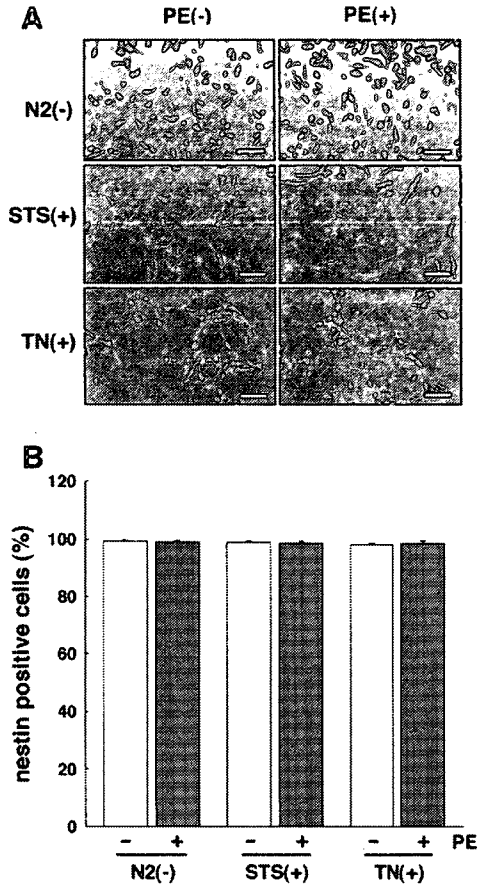

Fig. 5. Effect of phenylephrine on the proportion of nestin-positive cells under various stress conditions. Secondary cultured NPCs were exposed for 24 h to stress conditions without or with 10 μM phenylephrine: N2 deprivation medium, or exposure to 50 nM staurosporine (STS) or 30 ng/ml tunicamycin (TN). After 24 h, the NPCs were fixed and stained with anti-nestin and Hoechst. (A) Fluorescence microscopic images of cells labeled with anti-nestin (green) and Hoechst (blue). Scale bar=50 μm. (B) The percentages of nestin-positive cells in the cultures were quantified. No significant differences were seen among the groups.

untreated NPCs correlated with the difference in the amount of cell death. These results also indicated that phenylephrine protected NPCs from death during bFGF deprivation-induced stress. Moreover, we confirmed that α_1-adrenoceptor agonists specifically protected NPCs from death using another α_1-adrenoceptor agonist, cirazoline. Cirazoline treatment of NPCs under the same culture conditions resulted in a significant decrease in LDH release ($P<0.01$; Fig. 3C), indicating that α_1-adrenoceptor agonists promote survival of NPCs cultured in 1 ng/ml bFGF. A [^{3}H]thymidine incorporation assay showed that phenylephrine and cirazoline did not induce DNA synthesis of NPCs (data not shown).

3.4. α_1-adrenoceptor agonists prevent NPC death upon exposure to various stresses

To determine the extent to which α_1-adrenoceptor agonists could prevent NPC death, we employed other stress conditions: N2 deprivation, or exposure to 50 nM staurosporine or 30 ng/ml tunicamycin. The results of the LDH release assay for these stress conditions showed that N2 deprivation, staurosporine treatment, and tunicamycin treatment induced LDH release from NPCs (361±24%, 706±5% and 664±21%, respectively, relative to the controls; Fig. 4). However, application of the agonists to the NPC cultures under these stress conditions significantly reduced LDH release (N2 deprivation+phenylephrine, 238±18% $P<0.01$; N2

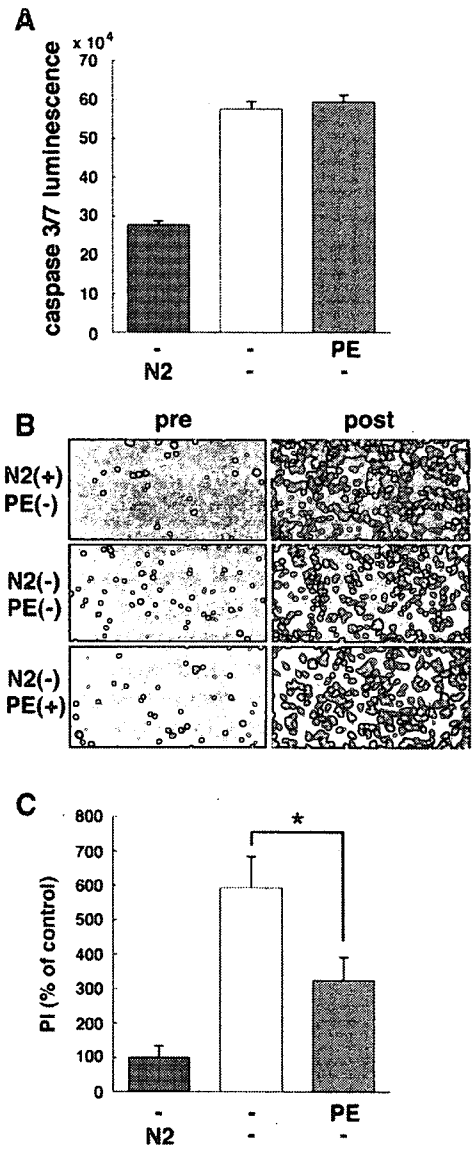

Fig. 6. Phenylephrine does not alter cellular caspase activity but changes propidium iodide penetration into NPCs. Secondary cultured NPCs were incubated without or with 10 μM phenylephrine (PE) under N2 deprivation conditions for 24 h. (A) Caspase-3 and caspase-7 activities in cell lysates were measured by luminometry. (B) Fluorescence microscopy images of dead cells stained with propidium iodide are presented (left). For positive controls, cells were fixed and stained with PI after permeabilization with 0.02% Triton X-100 (right). Scale bar=100 μm. (C) The intensity of propidium iodide staining was measured by fluorometry. Bars represent mean±S.E.M. ($n=4$). Significant differences are indicated by an asterisk (*$P<0.05$, Dunnett's test).